

Gaussian Pre-Activations in Neural Networks: Myth or Reality?

Pierre Wolinski

LAMSADE, Paris-Dauphine University, PSL University, CNRS, 75016 Paris, France

pierre.wolinski@dauphine.psl.eu

Julyan Arbel

Univ. Grenoble Alpes, Inria, CNRS, Grenoble INP, LJK, 38000 Grenoble, France

julyan.arbel@inria.fr

Reviewed on OpenReview: <https://openreview.net/forum?id=goe6fv6iSh>

Abstract

The study of feature propagation at initialization in neural networks lies at the root of numerous initialization designs. A very common assumption is that the pre-activations are Gaussian. Although this convenient *Gaussian hypothesis* can be justified when the number of neurons per layer tends to infinity, it is challenged by both theoretical and experimental work for finite-width neural networks. Our main contribution is to construct a family of pairs of activation functions and initialization distributions that ensure that the pre-activations remain Gaussian throughout the network depth, even in narrow neural networks, under the assumption that the pre-activations are independent. In the process, we discover a set of constraints that a neural network should satisfy to ensure Gaussian pre-activations. In addition, we provide a critical review of the claims of the Edge of Chaos line of work and construct a non-asymptotic Edge of Chaos analysis. We also propose a unified view on the propagation of pre-activations, encompassing the framework of several well-known initialization procedures. More generally, our work provides a principled framework for addressing the much-debated question: is it desirable to initialize the training of a neural network whose pre-activations are guaranteed to be Gaussian? Our code is available on GitHub: <https://github.com/p-wol/gaussian-preact/>.

Notations and vocabulary

Bold letters such as \mathbf{Z} , \mathbf{W} , \mathbf{B} , or \mathbf{x} , represent tensors of order larger or equal to 1. For a tensor $\mathbf{W} \in \mathbb{R}^{n \times p}$, we denote by $W_{ij} \in \mathbb{R}$ its component at the intersection of the i -th row and j -th column, $\mathbf{W}_i \in \mathbb{R}^{1 \times p}$ its i -th row and $\mathbf{W}_j \in \mathbb{R}^n$ its j -th column. Upper-case letters such as \mathbf{W} , X , Y , Z , or G , represent random variables. For a random variable Z , the function f_Z represents its density, F_Z its cumulative distribution function (CDF), S_Z its survival function, and ψ_Z its characteristic function. The *depth* of a neural network is its number of layers. The *width* of one layer is its number of neurons or convolutional units. The *infinite-width limit* of a neural network is the limiting case where the width of each layer tends to infinity.

1 Introduction

Let us take a neural network with L layers, in which every layer $l \in [1, L]$ performs the following operation:

$$\mathbf{X}^{l+1} := \phi(\mathbf{Z}^{l+1}), \quad (1)$$

$$\text{with: } \mathbf{Z}^{l+1} := \frac{1}{\sqrt{n_l}} \mathbf{W}^l \mathbf{X}^l + \mathbf{B}^l, \quad (2)$$

where $\mathbf{X}^{l+1} \in \mathbb{R}^{n_{l+1}}$ is its *activation*, $\mathbf{Z}^{l+1} \in \mathbb{R}^{n_{l+1}}$ its *pre-activation*, ϕ is the coordinate-wise *activation function*, $\mathbf{W}^l \in \mathbb{R}^{n_{l+1} \times n_l}$ is the *weight matrix* of the layer, $\mathbf{B}^l \in \mathbb{R}^{n_{l+1}}$ its *vector of biases*, and $\mathbf{X}^l \in \mathbb{R}^{n_l}$ its

input (also the preceding layer activation). This paper focuses on the distribution of the pre-activations \mathbf{Z}^l as l grows, for a fixed input \mathbf{x} , and weights \mathbf{W}^l and biases \mathbf{B}^l randomly sampled from known distributions.

Recurring questions arise in both Bayesian deep learning and in parameter initialization procedures: How to choose the distribution of the parameters $\mathbf{W}^l, \mathbf{B}^l$ and according to which criteria, and how should the distribution of the pre-activations \mathbf{Z}^l look like? Answering these questions is fundamental to finding efficient ways of initializing neural networks, that is, appropriate distributions for \mathbf{W}^l and \mathbf{B}^l at initialization. In Bayesian deep learning, this question is related to the search for a suitable prior, which is still a topic of intense research (Wenzel et al., 2020, Fortuin et al., 2022, Fortuin, 2022, Arbel et al., 2024, Papamarkou et al., 2024).

Initialization strategies. A whole line of work in the field of initialization strategies for neural networks is based on preserving the statistical characteristics of the pre-activations as they propagate into a network. In short, the input of the neural network is assumed to be fixed, while all the parameters are considered to be randomly drawn, according to a candidate initialization distribution. Then, by using heuristics, some statistical characteristics of the pre-activations are deemed desirable. Finally, these statistical characteristics are propagated to the initialization distribution, which indicates how to choose it.

For instance, one of the first results of this kind, proposed by Glorot & Bengio (2010), is based on the preservation of the variance of both the pre-activations and the backpropagated gradients across the layers of the neural network. The resulting constraint on the initialization distribution of the weights \mathbf{W}^l is about its variance: $\text{Var}(W_{ij}^l/\sqrt{n_l}) = 2/(n_l + n_{l+1})$.¹ Then, He et al. (2015) have refined this idea by taking into account the nonlinear deformation of the pre-activations by the activation function. They also showed that the inverted arithmetical average $2/(n_l + n_{l+1})$, resulting from a compromise between the preservation of variance during both propagation and backpropagation, can be changed into $1/n_l$ or $1/n_{l+1}$ with negligible impact on the neural network.² Notably, with $\phi(x) = \text{ReLU}(x) := \max(0, x)$, they obtain $\text{Var}(W_{ij}^l) = 2/n_l$, where the factor 2 is meant to compensate for the loss of information due to the fact that ReLU is zero on \mathbb{R}^- . We summarize and compare several initialization strategies in Table 1 (Section 3.4)

Edge of Chaos (EOC). After the studies revolving around initialization, Poole et al. (2016) and Schoenholz et al. (2017) focused on the correlation between the pre-activations of two data points \mathbf{x}_a and \mathbf{x}_b . By preserving this correlation when propagating the inputs into the neural network, information about the geometry of the input space is meant to be preserved. Thus, training the weights is meaningful at initialization, regardless of their positions in the network. This heuristic is finer than the previous ones, since attention is paid to the correlation between pre-activations and their variance (a joint criterion is used instead of a marginal one). The range of valid initialization distributions is modified accordingly, with a relation between $\sigma_w^2 = \text{Var}(W_{ij}^l)$ and $\sigma_b^2 = \text{Var}(B_i^l)$ that should be ensured. This specific relationship is referred to as the *Edge of Chaos* (EOC).

Finally, it is worth mentioning the work of Hayou et al. (2019), in which the usual claims about the EOC initialization are tested with several choices of activation functions. Notably, the authors have run a large series of experiments in order to check whether the intuition behind the EOC initialization leads to better performance after training. Also, at the opposite of finding an initialization distribution for the parameters, Klambauer et al. (2017) focused on tuning the parameters of the activation function (leading to the SELU activation function). As in the preceding techniques, they aim for variance-preserving layers.

In the following, the term “Edge of Chaos” is used in two different manners: “EOC framework”, “EOC formalism”, or “EOC theory” refer to a setup where input data points are deterministic and weights and biases are random, whereas in the context of initialization of weights and biases, “EOC” alone refers to a specific set of pairs (σ_w^2, σ_b^2) matching a given theoretical condition (Point 2, see Section 3.1).

Bayesian prior and initialization distribution. There exists a close relationship between the initialization distribution in deterministic neural networks and the prior distribution in Bayesian neural networks. For

¹In the original paper, the considered weight matrix is $\tilde{\mathbf{W}}^l := \mathbf{W}^l/\sqrt{n_l}$, so $\text{Var}(\tilde{W}_{ij}^l) = 2/(n_l + n_{l+1})$.

²More generally, any choice of the form $1/(n_l^\alpha n_{l+1}^{1-\alpha})$ with $\alpha \in [0, 1]$ is valid, as long as the same α is used for all layers.

instance, let us use variational inference to approximate the Bayesian posterior of the parameters of a neural network (Graves, 2011). In this case, the Bayesian posterior is approximated sequentially by performing a gradient descent over the so-called “variational parameters” (Hoffman et al., 2013). This technique requires to backpropagate the gradient of the loss through the network, as when training deterministic networks. Therefore, as with the initialization distribution, the prior distribution must be constructed in such a way that the input and the gradient of the loss propagate and backpropagate correctly (Sec. 2.2, Ollivier, 2018; Chap. 2, Neal, 1996).

Gaussian hypothesis for the pre-activations. In the context of random weights and biases, we call the *Gaussian hypothesis* the assumption that all the pre-activations Z_i^l are Gaussian random variables, at any layer l and for any neuron i . This hypothesis is common in the theoretical analysis of the properties of neural networks at initialization. Specifically, this is a fundamental assumption when studying the “Neural Tangent Kernels” (NTK) (Jacot et al., 2018) or Edge of Chaos (Poole et al., 2016). In a nutshell, the NTK is an operator describing the optimization trajectory of an *infinitely wide* neural network (NN), which is believed to help understand the optimization of ordinary NNs. On one side, this Gaussian hypothesis can be justified in the case of “infinitely wide” NNs (i.e., when the widths n_l of the layers tend to infinity), by application of the Central Limit Theorem (Matthews et al., 2018). On the other side, this Gaussian hypothesis is apparently necessary to get the results of the EOC and NTK lines of work. However, it remains debated for both theoretical and practical reasons.

First, from a strictly theoretical point of view, it has been shown that, for finite-width NNs (finite n_l), the distribution of Z_i^l has heavier tails as l increases, that is, as information flows from the input to the output (Vladimirova et al., 2019; 2021). Second, a series of experiments tend to show that pushing the distribution of the pre-activations towards a Gaussian (e.g., through a specific Bayesian prior) leads to worse performances than pushing it towards distributions with heavier tails, e.g., Laplace distribution (Fortuin et al., 2022).

Besides, the condition under which the Gaussian hypothesis remains valid is an important source of confusion. As an example, Sitzmann et al. (2020) state that: “for a uniform input in $[-1, 1]$, the [pre-]activations throughout a SIREN³ are standard normal distributed [...], irrespective of the depth of the network, if the weights are distributed uniformly in the interval $[-c, c]$ with $c = \sqrt{6}/n_l$ in each layer $[l]$.” (Theorem 1.8, Appendix 1.3). Though this formal statement seems to hold for all layers and whatever their widths, it is only an asymptotic result, since it uses the Central Limit Theorem in its proof. Consequently, this theorem is not usable in practical SIRENs, since it does not provide any speed of convergence of the distribution of the pre-activations to a Gaussian, as each n_l tends to infinity.⁴

Deviation from the Gaussian distribution in the finite-width case. More recently, several attempts have been made to characterize the distribution of the pre-activations in the finite-width case. In particular, Yaida (2020), Balasubramanian et al. (2024), Trevisan (2023), Basteri & Trevisan (2024), Favaro et al. (2025) provide bounds on the discrepancy between the actual distribution of the pre-activations in the finite-width case and the Gaussian limit in the infinite-width case. One may also refer to Roberts et al. (2022) for a complete study. Although these works provide results for finite-widths networks, they only apply when the widths are large. Additionally, Vladimirova et al. (2019; 2021) show that for finite-width NNs, the pre-activation distribution gets heavier-tailed when getting deeper into the neural network. From another point of view, Noci et al. (2021) provides an analytical expression is provided for the distribution of the pre-activations, but only in terms of Meijer-G functions (Erdélyi et al., 1953), which are difficult to manipulate.

Addressing the limitations of the EOC analysis. Preserving the shape of the distribution of the pre-activations is a key assumption of the EOC works. This assumption is usually justified if we assume that the considered network is in the NTK regime, which means that the layer widths are large enough to ensure that the Neural Tangent Kernel is constant throughout training. However, this assumption is generally not

³Sinusoidal representation network.

⁴According to Matthews et al. (Th. 4, 2018), the pre-activations tend to become Gaussian irrespective of the growth rates of each n_l , so Theorem 1.8 of Sitzmann et al. (2020) is *asymptotically true for all layers and all growth rates of each n_l* . But this result still does not provide any convergence speed.

true and has been discussed in several papers. For instance, Hanin & Nica (2020) showed that if the ratio depth/width does not tend to zero, the NTK varies significantly during training. This illustrates that the NTK is unlikely to be constant during training for narrow and deep neural networks. This phenomenon has also been observed empirically by Seleznova & Kutyniok (2022).

In parallel, another limitation of the EOC has been spotted: with the EOC initialization scheme, the correlation between the pre-activations given by two different outputs tends to a unique real number, independent of the input data. Therefore, the EOC initialization inevitably leads to degenerate correlations in deeper layers, which means that the geometry of the input space is progressively forgotten during propagation. This phenomenon has been studied extensively by Martens et al. (2021), and Martens et al. (2021), Zhang et al. (2022) solve this problem with an innovative solution: transform the activation function in order to “shape” the kernel.

This idea of “kernel shaping” through a transformation of the activation function has then been used by Li et al. (2022) to solve both issues presented above: the NTK regime does not hold in practice, and the EOC initialization leads to degenerate correlations. So, Li et al. (2022) have proposed to take into account the $O(1/\sqrt{n})$ deviation from the infinite-width limit $n \rightarrow \infty$. This results in a set of modifications of the activation functions that are adapted to n and, therefore, are also dependent on n .

Motivation. In the works cited above, the general problem is to control the distribution of pre-activations, mostly in order to design good initialization strategies. To this end, two approaches have been used: 1. describing analytically this distribution with given activation functions (e.g., Noci et al., 2021, Favaro et al., 2025); 2. tuning the activation function to make the pre-activation match a given property (e.g., Zhang et al., 2022, Li et al., 2022). In the current work, we take approach 2. by constructing activation functions and initialization distributions to provide Gaussian pre-activation at initialization, *without relying on the infinite-width limit hypothesis or any asymptotic expansion around that limit*.

The starting point of our study is the original EOC works (Schoenholz et al., 2017, Poole et al., 2016), which rely only on the preservation of the shape of the pre-activations. This behavior is usually justified by the central limit theorem in the infinite-width limit, which is one of the main assumptions in the works cited above. The direction we explore in this paper is different: we study the shape of the distributions of the pre-activations themselves.

So, we first measure the Gaussianity of the pre-activations. Since the EOC relies on the assumption that the pre-activations are Gaussian, it is necessary to check it experimentally and directly, regardless of how close our neural network is to the NTK regime (i.e., infinite-width limit). Second, as Martens et al. (2021), Zhang et al. (2022), Li et al. (2022), we propose to construct new activation functions. Gaussianity is preserved. But, unlike these works, we focus on the Gaussianity of the pre-activations, so we do not rely on the infinite-width limit hypothesis or any asymptotic expansion around that limit. To do so, we study individual weights, and, unlike Li et al. (2022), the resulting activation functions do not depend on the width of the neural network. This approach explicitly allows the study of very narrow neural networks, regardless of the depth.

More generally, the goal of the series of articles presented above, of which this one is a part, is to propose a principled framework for studying the neural networks at initialization, while proposing initialization schemes and activation functions to solve problems we may encounter at initialization. To study the distribution of the pre-activations in detail, several strategies can be used. As explained in Section 2, such a study is very difficult to achieve for arbitrary activation functions. Moreover, these studies are based on deviations from the infinite-width limit (Yaida, 2020, Balasubramanian et al., 2024, Favaro et al., 2025). The strategy we adopt in this paper is the opposite: we construct activation functions that, by design, should lead to pre-activations whose distribution is known.

Contributions. Therefore, we present in this paper a new framework for studying neural networks at initialization and propose new families of initialization distributions and activation functions. In particular, to obtain results that are independent of how close we are to the NTK regime, we focus on the distribution of the pre-activations during propagation. First, we experimentally test their Gaussianity, i.e., whether the *Gaussian hypothesis* holds or not. We show that it does not hold in many cases. Second, we construct

families of activation functions and initialization distributions to make this Gaussian hypothesis hold, and we show their construction process. Since this process is flexible and can be used to construct other activation functions, it is a contribution in itself.

To be more specific:

- we experimentally demonstrate that the Gaussian hypothesis is mostly invalid in multilayer perceptrons with finite width (Section 3.1 and Section 3.2);
- contrary to a claim of Poole et al. (2016) and usual practical results in the EOC framework, we show in Proposition 2 that the variance of the pre-activations does not always have at most one nonzero attraction point; we provide an example of an activation function for which the number of such attraction points is infinite (Section 3.3);
- we propose a unified view on pre-activations propagation, encompassing the framework of several well-known initialization procedures (Section 3.4);
- we deduce a set of constraints that the activation function and the initialization distribution of weights and biases must fulfill to guarantee Gaussian pre-activations at initialization under a pre-activations' independence assumption – including with finite-width layers (Section 4.1 and Section 4.2);
- we propose new families of activation functions, denoted by $(\phi_\theta^o)_\theta$ and $(\phi_\theta^p)_\theta$, and initialization distributions designed to achieve this goal of Gaussian pre-activations at initialization (Section 4.3 and Section 4.4);
- we empirically demonstrate that, with our activation functions $(\phi_\theta^p)_\theta$, the distribution of the pre-activations remains Gaussian during propagation, while it drifts away from the standard Gaussian when using tanh and ReLU (Sections 5.1 and 5.2);
- we show that, overall, when training very narrow and deep networks, the usual setups with tanh or ReLU activation functions and EOC initialization lead to worse performance than with our activation functions $(\phi_\theta^o)_\theta$ (Section 5.4).

Additionally, we train, evaluate and compare neural networks built according to our family of activation functions and initialization distributions, and usual ones (tanh or ReLU, Gaussian EOC initialization).

Summary of the paper. We begin by reviewing the widely used assumptions about pre-activations in Section 2. Then, we make in Section 3 a critical review of several results about pre-activations propagation in a neural network: the discussion, additional experiments, and the criticism we are proposing, particularly in the EOC line of works, are the foundations of our contributions. In Section 4, we propose a new family of activation functions, along with a family of initialization distributions. They are defined so as to ensure that the pre-activations distribution propagates without deformation across the layers, including with networks that are far from the “infinite-width limit”. More specifically, we ensure that the pre-activations remain Gaussian at any layer, and we provide a set of constraints that the activation function and the initialization distribution of the parameters should match to attain this goal, under a pre-activations' independence assumption. Finally, we propose in Section 5 a series of simulations in order to check whether our propositions meet the requirement of maintaining Gaussian pre-activations across neural networks. We also show the performance of trained neural networks in different setups, including standard ones and the one we are proposing.

2 Common assumptions about pre-activations

Several attempts have been made to provide an accurate description of the pre-activations at initialization.

Neural networks as Gaussian processes. A line of works, initiated by Neal (1996), has focused on the study of the pre-activations of neural networks on their infinite-width limit, that is, the limit of infinite number of neurons per layer. Notably, it has been proven (Matthews et al., 2018, Lee et al., 2018) that the outputs and the pre-activations of a randomly initialized neural network tend to a Gaussian process with known mean and covariance. The proof can be achieved by using the fact that the pre-activations of the same layer are exchangeable random variables, making it possible to use a variation of the central limit theorem at each layer. These first results have led to the development of the Neural Tangent Kernel framework (Jacot et al., 2018, Lee et al., 2019, Arora et al., 2019c), which allows us to study the full optimization trajectory of a neural network trained by gradient descent (Du et al., 2019, Allen-Zhu et al., 2019, Arora et al., 2019b).

Despite the significance of these convergence results, the discussion about the practicality of their hypotheses is still active, notably about the infinite number of neurons per layer and the linear training dynamic. Besides, two essential by-products of these hypotheses are subject to discussion: the fact that the pre-activations are *Gaussian* and *independent* in the infinite-width limit.

Assumption of independent pre-activations. The assumption that pre-activations of the same layer are independent is very common in the literature on neural networks' initialization. For instance, this assumption is explicitly made in He et al. (2015). In the Edge of Chaos literature, the pre-activations of the same layer are implicitly assumed to be independent (Poole et al., 2016, Schoenholz et al., 2017): at a given layer, the vector of pre-activations is assumed to be a Gaussian vector with a diagonal covariance, which implies independence. More broadly, as soon as the infinite-width limit is taken, the pre-activations tend to Gaussian processes with zero covariance between pre-activations of the same layer (Matthews et al., 2018, Jacot et al., 2018), that is independence.

3 Propagating pre-activations

In this section, we propose a critical review of several aspects of the Edge of Chaos framework. We recall the fundamental ideas of the EOC in Section 3.1. In Section 3.2, we perform some experiments at the initialization of a multilayer perceptron, in which we propagate data points sampled from CIFAR-10. These results illustrate a limitation of the EOC framework when using neural networks with a small number of neurons per layer. Then, we build in Section 3.3 an activation function such that the variance of the propagated pre-activations admits an infinite number of stable fixed points, which is a counterexample to a claim of Poole et al. (2016). Finally, we propose in Section 3.4 a unified representation of several initialization procedures.

3.1 Propagation of the correlation between data points

Edge of Chaos (EOC) framework. In the EOC line of work, the inputs of the neural network are supposed to be fixed, while the weights and biases are random. In order to study the propagation of the distribution of the pre-activations \mathbf{Z}^l , Poole et al. (2016) and Schoenholz et al. (2017) propose to study two quantities:

$$v_a^l := \mathbb{E}[(Z_{j;a}^l)^2], \quad (3)$$

$$c_{ab}^l := \frac{1}{\sqrt{v_a^l v_b^l}} \mathbb{E}[Z_{j;a}^l Z_{j;b}^l], \quad (4)$$

where $Z_{j;a}^l$ is the j -th coordinate of the vector \mathbf{Z}_a^l of pre-activations before layer l , when the input of the neural network is a data point \mathbf{x}_a . The expectation is computed over the full set of the parameters, i.e., weights and biases. So, we can interpret v_a^l as the variance of the pre-activations of a data point \mathbf{x}_a , and c_{ab}^l as the correlation between the pre-activations of two data points \mathbf{x}_a and \mathbf{x}_b , over random initializations of the parameters, distributed independently in the following way:

$$W_{ij}^l \sim P_w(\sigma_w) \quad \text{with} \quad \mathbb{E}[W_{ij}^l] = 0 \quad \text{and} \quad \text{Var}(W_{ij}^l) = \sigma_w^2, \quad (5)$$

$$B_i^l \sim P_b(\sigma_b) \quad \text{with} \quad \mathbb{E}[B_i^l] = 0 \quad \text{and} \quad \text{Var}(B_i^l) = \sigma_b^2. \quad (6)$$

Remark 1. Since the parameters are sampled independently with zero-mean, then:

$$\mathbb{E}[Z_{j_1;a}^l Z_{j_2;a}^l] = v_a^l \delta_{j_1 j_2}, \quad (7)$$

$$\frac{1}{\sqrt{v_a^l v_b^l}} \mathbb{E}[Z_{j_1;a}^l Z_{j_2;b}^l] = c_{ab}^l \delta_{j_1 j_2}. \quad (8)$$

This is why Definitions (3) and (4) do not depend on j , and the crossed terms in j_1 and j_2 are not worth studying (they are zero).

Remark 2. The distributions of W_{ij}^l and B_i^l considered by [Poole et al. \(2016\)](#) and [Schoenholz et al. \(2017\)](#) are normal with zero-mean, that is:

$$P_w(\sigma_w) = \mathcal{N}(0, \sigma_w^2) \quad \text{and} \quad P_b(\sigma_b) = \mathcal{N}(0, \sigma_b^2).$$

We loosen this assumption in (5) and (6), where we assume that these random variables are zero-mean with a variance we can control. Their theoretical claim remains valid under this broader assumption.

Theoretical analysis. Given two fixed inputs \mathbf{x}_a and \mathbf{x}_b , the goal of the EOC theory is to study the propagation of the correlation c_{ab}^l of $Z_{j;a}^l$ and $Z_{j;b}^l$ which goes as follows ([Poole et al., 2016](#), [Schoenholz et al., 2017](#)):

1. build recurrence equations for $(c_{ab}^l)_l$ of the form: $c_{ab}^{l+1} = f(c_{ab}^l)$;
2. describe the dynamics of $(c_{ab}^l)_l$;
3. provide a procedure to compute the variance of the weights' and biases' distributions such that $(c_{ab}^l)_l$ tends to 1 with a sub-exponential rate (instead of an exponential rate).

Point 1: recurrence equations. Point 1 is achieved by using the Gaussian hypothesis for the pre-activations. That is, the distribution of the pre-activations \mathbf{Z}^l is assumed to be Gaussian, whatever the layer l and its width n_l . The recurrence equations define a variance map \mathcal{V} and a correlation map \mathcal{C} as follows:

$$v_a^{l+1} = \mathcal{V}(v_a^l | \sigma_w, \sigma_b) := \sigma_w^2 \int \phi\left(\sqrt{v_a^l} z\right)^2 \mathcal{D}z + \sigma_b^2 \quad (9)$$

$$c_{ab}^{l+1} = \mathcal{C}(c_{ab}^l, v_a^l, v_b^l | \sigma_w, \sigma_b) := \frac{1}{\sqrt{v_a^{l+1} v_b^{l+1}}} \left[\sigma_w^2 \int \phi\left(\sqrt{v_a^l} z_1\right) \phi\left(\sqrt{v_b^l} z_2'\right) \mathcal{D}z_1 \mathcal{D}z_2 + \sigma_b^2 \right], \quad (10)$$

$$\text{where } z_2' := c_{ab}^l z_1 + \sqrt{1 - (c_{ab}^l)^2} z_2, \quad \text{and} \quad \mathcal{D}z := \frac{1}{\sqrt{2\pi}} \exp\left(-\frac{z^2}{2}\right) dz. \quad (11)$$

These equations are approximations of the true information propagation dynamics, which involves necessarily the number of neurons n_l per layer. Actually, passing a Gaussian vector \mathbf{Z}^l through a layer with random Gaussian weights and biases produces a pre-activation \mathbf{Z}^{l+1} with a distribution which is difficult to describe. On one side, as the dimension n_l of the input \mathbf{Z}^l tends to infinity, the Central Limit Theorem (CLT) applies, and the output \mathbf{Z}^{l+1} tends to become Gaussian.⁵ The assumption that the components of \mathbf{Z}^{l+1} are Gaussian is referred to as the *Gaussian hypothesis*. On the other side, with finite n_l , the tail of the distribution of \mathbf{Z}^{l+1} has been proven to become heavier than the Gaussian one, both theoretically ([Vladimirova et al., 2019](#); [2021](#)) and experimentally (see Section 3.2).

Finally, by assuming that $(v_a^l)_l$ and $(v_b^l)_l$ have already converged to the same limit $v^* \neq 0$ as $l \rightarrow \infty$, it is possible to rewrite Equation (10) in a nicer way:

$$c_{ab}^{l+1} = \mathcal{C}_*(c_{ab}^l) := \mathcal{C}(c_{ab}^l, v^*, v^* | \sigma_w, \sigma_b). \quad (12)$$

Now that the dynamics of $(c_{ab}^l)_l$ is written in the form $c_{ab}^{l+1} = \mathcal{C}_*(c_{ab}^l)$, it becomes sufficient to plot \mathcal{C}_* to study its convergence. The two hypotheses made, i.e., the Gaussian one and the instant convergence of $(v_a^l)_l$ and $(v_b^l)_l$ to a unique nonzero limit v^* , are fundamental to obtaining the simple equation of evolution (12).

⁵Even if the coordinates Z_j^l are dependent, the CLT is still valid, as proven by [Matthews et al. \(2018\)](#) by using properties of exchangeable random variables ([De Finetti, 1937](#)).

Point 2: dynamics of the correlation through the layers. Then, Point 2 can be achieved. Now that the trajectory of $(c_{ab}^l)_l$ is determined only by the function \mathcal{C}_* , it becomes easy to find numerically its limit c^* and its rate of convergence. Specifically, we can distinguish three possible cases:

- *chaotic phase*: $\lim_{l \rightarrow \infty} c_{ab}^l = c^* < 1$. The correlation between $Z_{j;a}^l$ and $Z_{j;b}^l$ tends to a constant that is strictly less than 1. So, even if $Z_{j;a}^1$ and $Z_{j;b}^1$ are highly correlated (which means that \mathbf{x}_a and \mathbf{x}_b are close to each other), they tend to decorrelate when going deeper in the network;
- *ordered phase*: $\lim_{l \rightarrow \infty} c_{ab}^l = c^* = 1$ with $\mathcal{C}'_*(1) < 1$ (the prime here denotes the derivative of a function). The correlation between $Z_{j;a}^l$ and $Z_{j;b}^l$ tends to 1 with an exponential rate, including when $Z_{j;a}^1$ and $Z_{j;b}^1$ are almost fully decorrelated;
- *edge of chaos*: $\lim_{l \rightarrow \infty} c_{ab}^l = c^* = 1$ with $\mathcal{C}'_*(1) = 1$. The correlation between $Z_{j;a}^l$ and $Z_{j;b}^l$ tends to 1 with a sub-exponential rate, including when $Z_{j;a}^1$ and $Z_{j;b}^1$ are almost fully decorrelated.

Point 3: best choices for the initialization distribution. Poole et al. (2016) and Schoenholz et al. (2017) claim that pairs (σ_w^2, σ_b^2) which lead either to the chaotic phase or the ordered phase should be avoided. In both cases, we expect that information contained in the propagated data (or the backpropagated gradients) would vanish at an exponential rate. So, we want to find pairs (σ_w^2, σ_b^2) lying “at the edge of chaos”, that is, making the sequence $(c_{ab}^l)_l$ converge to 1 at a sub-exponential rate. The *Edge of Chaos initializations* are the initialization distributions of the weights and the biases such that the pair of variances (σ_w^2, σ_b^2) lies at the Edge of Chaos.

Remark 3. *Even in the favorable edge of chaos configuration, the sequence of correlations $(c_{ab}^l)_l$ tends to 1, whatever the data points \mathbf{x}_a and \mathbf{x}_b . So a loss of information at initialization seems unavoidable in very deep networks.*

If one wants to create an initialization procedure with a smaller information loss, it becomes reasonable to consider data-dependent initialization schemes (i.e., a warm-up phase before training). Such an initialization strategy has been sketched by Mao et al. (2021), who make use of the “Information Bottleneck” formalism (Tishby, 1999, Shwartz-Ziv & Tishby, 2017, Saxe et al., 2019).

Strengths and weaknesses of the Edge of Chaos framework. One key feature of the Edge of Chaos framework is the simplicity of the recurrence equation (12): it involves only the correlation c_{ab}^l as a variable, and all other parameters (such as v_a^l and v_b^l) are assumed to be fixed once and for all. Notably, in Equation (10), the computation of c_{ab}^{l+1} involves the distribution of the pre-activations outputted by layer l , which is assumed to be $\mathcal{D} = \mathcal{N}(0, 1)$. In other words, the distribution \mathcal{D}^l of the pre-activations \mathbf{Z}^l is assumed to be constant and equal to \mathcal{D} . However, in neural networks with finite widths, \mathcal{D}^l is not constant and evolves according to a propagation equation:

$$\mathcal{D}^{l+1} \text{ is the distribution of } \mathbf{Z}^{l+1} = \frac{1}{\sqrt{n_l}} \mathbf{W}^l \phi(\mathbf{Z}^l) + \mathbf{B}^l, \text{ where } \mathbf{Z}^l \sim \mathcal{D}^l. \quad (13)$$

Such an equation involves a sum of products of random variables, which is usually difficult to keep track of.⁶ Though Noci et al. (2021) have proposed an analytical procedure to compute the \mathcal{D}^l explicitly, it works only for networks with ReLU or linear activation functions, and involves Meijer G-functions (Erdélyi et al., 1953), which are difficult to handle numerically.

3.2 Results on realistic datasets

As far as we know, there does not exist any experimental result about the propagation of the correlations with a non-synthetic dataset and a finite-width neural network. We propose to visualize in Figure 1 the propagation of correlation c_{ab}^l with dataset CIFAR-10 (results on MNIST are reported in Appendix H.1), in the case of the multilayer perceptron with various numbers of neurons per layer n_l (i.e., widths). Then, we show in Figure 2 the distance between the standardized distribution of the pre-activations and the standard Gaussian $\mathcal{N}(0, 1)$.

⁶For instance, a product of two Gaussian random variables is not Gaussian.

Propagation of the correlations. First, we have sampled randomly 10 data points in each of the 10 classes of the CIFAR-10 dataset, that is 100 in total for each dataset. Then, for each tested neural network (NN) architecture, we repeated $n_{\text{init}} = 1000$ times the following operation: (i) sample the parameters according to the EOC;⁷ (ii) propagate the 100 data points in the NN. Thereafter, for each pair $(\mathbf{x}_a, \mathbf{x}_b)$ of the selected 100 data points, we have computed the empirical correlation c_{ab}^l between the obtained pre-activations, averaged over the n_{init} samples. Finally, we have averaged the results over the classes: the matrix C_{pq}^l plotted in Figure 1 shows the mean of the correlation c_{ab}^l for data points \mathbf{x}_a and \mathbf{x}_b belonging respectively to classes p and q in $\{0, \dots, 9\}$.⁸ Only the experiments with CIFAR-10 are reported in Figure 1; the results on MNIST, which are similar, are reported in Figure 14 in Appendix H.1.

In accordance with the theory of the EOC, we observe in Figure 1 that the average correlation between pre-activations tends to 1, except in the case $\phi = \text{ReLU}$ and $n_l = 10$. In this case, it is not even clear that the sequences of correlations $(C_{pq}^l)_l$ converge at all, since some inter-class correlations are lower at $l = 30$ than $l = 10$, while we expected them to grow until 1. There is also a difference between activation functions tanh and ReLU: the convergence to 1 seems to be much quicker with $\phi = \text{ReLU}$ than with $\phi = \text{tanh}$, when $n_l = 100$.

We observe that the rate of convergence of $(C_{pq}^l)_l$ towards 1 not only varies with the NN width n_l but also varies in different directions depending on the activation function. When n_l grows from 10 to 100, the convergence of $(C_{pq}^l)_l$ to 1 slows down with $\phi = \text{tanh}$, while it accelerates with $\phi = \text{ReLU}$. Since this striking inconsistency with the EOC theory is related to n_l , it is due to the “infinite-width” approximation, precisely made to eliminate the dependency on n_l in the recurrence Equations (9) and (10), and consequently simplify them.

Remark 4. According to the framework of the EOC, the inputs \mathbf{x}_a and \mathbf{x}_b are assumed to be fixed. So, it is improper to define a correlation c_{ab}^0 between \mathbf{x}_a and \mathbf{x}_b . However, when considering the correlation c_{ab}^1 of the pre-activations right after the first layer, the empirical correlation between inputs \mathbf{x}_a and \mathbf{x}_b appears naturally:

$$c_{ab}^1 = \sigma_w^2 \cdot \frac{\mathbf{x}_a^T \mathbf{x}_b}{n} + \sigma_b^2, \quad (14)$$

where $\hat{c}_{ab}^0 := \mathbf{x}_a^T \mathbf{x}_b / n$ plays the role of an empirical correlation between \mathbf{x}_a and \mathbf{x}_b , assuming that the empirical mean and variance of both \mathbf{x}_a and \mathbf{x}_b are respectively 0 and 1.⁹

Propagation of the distances to the Gaussian distribution. We test in Figure 2 the Gaussian hypothesis in a multilayer perceptron of $L = 100$ layers, with a constant width $n_l \in \{10, 100, 1000\}$, and an activation function $\phi \in \{\text{ReLU}, \text{tanh}\}$. We propagate a single point sampled from the CIFAR-10 dataset, and we compute the empirical distribution of the pre-activations by drawing 10000 samples of the parameters of the neural network.

In Figure 2, we plot the Kolmogorov–Smirnov statistic of the standardized pre-activations for each layer, and we compare it to a threshold corresponding to a p -value of 0.05. Thus, according to Figure 2, the Gaussian hypothesis is rejected with a p -value of 0.05 for the ReLU activation function in all considered setups ($n_l \in \{10, 100, 1000\}$), and it is rejected too for the tanh activation function in the narrow network setup ($n_l = 10$).

We provide all the details about the Kolmogorov–Smirnov test in Appendix G, and additional details and experiments in the multilayer perceptron setup in Section 5.2.

⁷For the tanh activation function, a study of the EOC can be found in Poole et al. (2016). For ReLU, the EOC study is more subtle and can be found in Hayou et al. (2019).

⁸Correlations c_{ab}^l with $a = b$ have been excluded from the computation to show the intra-class correlation between *different* samples.

⁹Usually, this assumption does not hold exactly: it is common to normalize the entire dataset in such a way that the whole set of the features of all training data points has empirical mean 0 and variance 1, but not each data point individually. See also Definition 5.

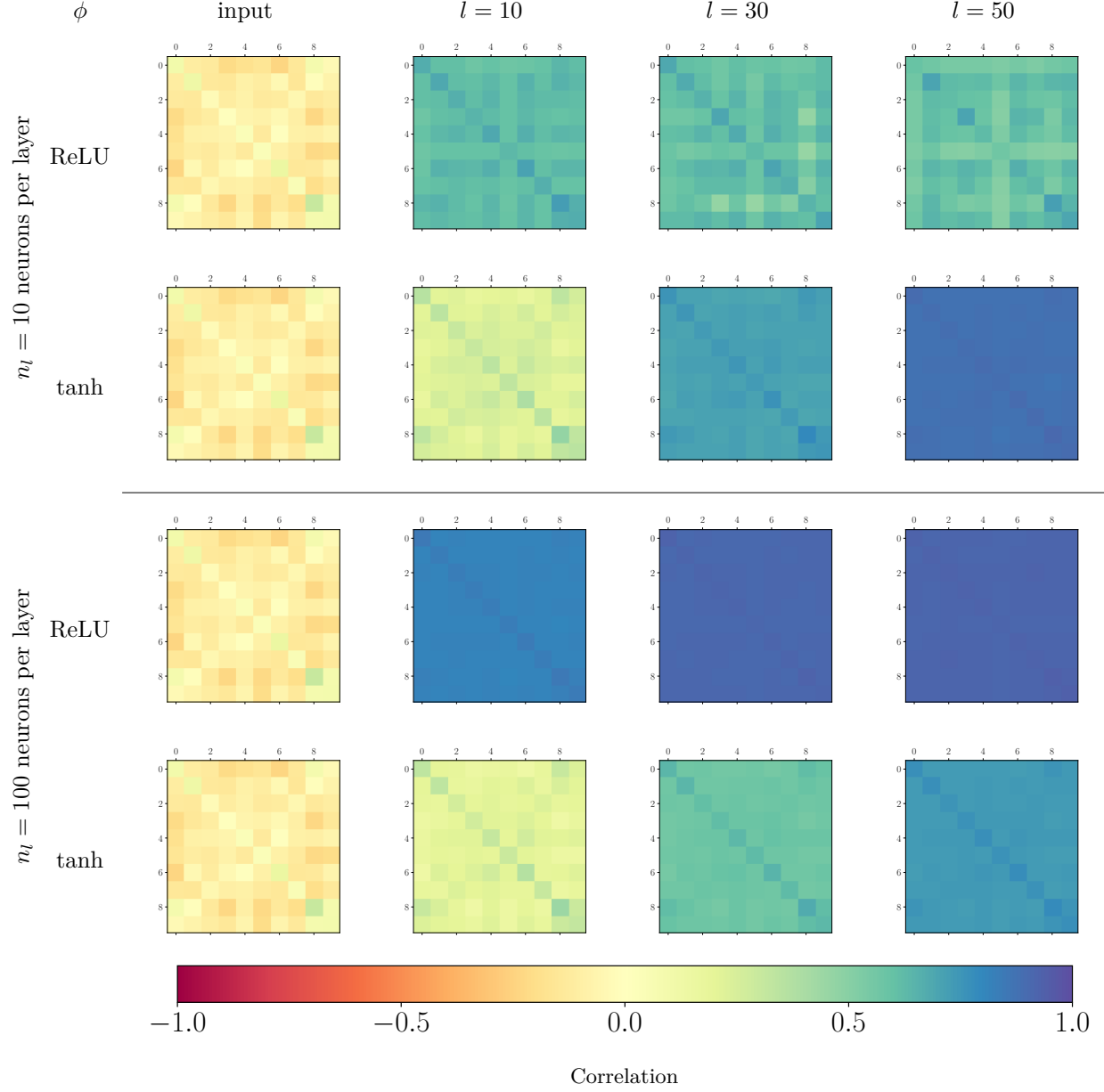


Figure 1: Propagation of correlations c_{ab}^l in a multilayer perceptron with activation function $\phi \in \{\tanh, \text{ReLU}\}$ and inputs sampled from the CIFAR-10 dataset. According to the EOC claims, they should tend to 1 as $l \rightarrow \infty$. Each plot displays a 10×10 matrix C_{pq}^l whose entries are the average correlation between the pre-activations propagated by samples from classes $p, q \in \{0, \dots, 9\}$, at the input and right after layers $l \in \{10, 30, 50\}$. See Fig. 14, App. H.1, for results on MNIST.

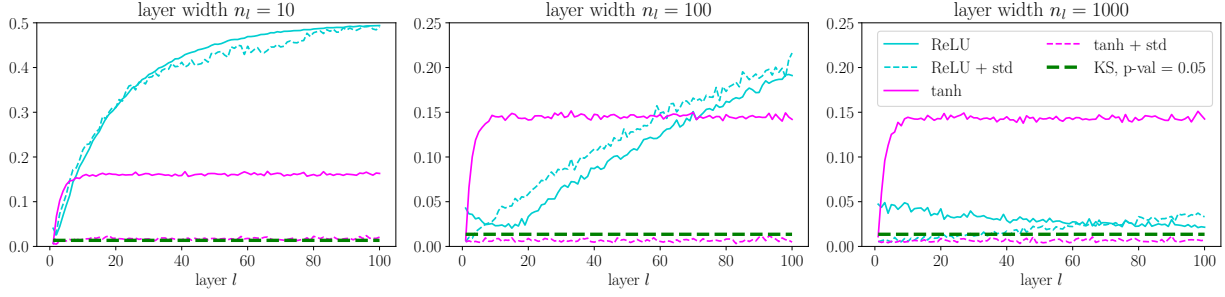


Figure 2: Evolution of the \mathcal{L}^∞ -distance between the standard Gaussian $\mathcal{N}(0, 1)$ and: (solid line) the empirical CDF of the pre-activations; (dotted line) the the empirical CDF of the standardized pre-activations. This distance should remain close to zero if the pre-activations are Gaussian. The empirical CDF of \mathcal{D}^l have been computed with 10000 samples. The green dotted line corresponds to the threshold given by the Kolmogorov–Smirnov test with a p -value of 0.05: any point above it corresponds to a distribution for which the Gaussian hypothesis should be rejected with a p -value of 0.05.

3.3 Convergence of the sequence of variances $(v_a^l)_l$

Multiple stable limits. As reminded in Point 1, Section 3.1, it is a key assumption of the EOC formalism to assume that, whatever the starting point v_a^0 , the sequence $(v_a^l)_l$ converges to the same limit v^* as $l \rightarrow \infty$. As far as we know, no configuration where the map \mathcal{V} has two nonzero stable points or more has been encountered in past works. Moreover, it is believed that such configurations do not exist, as stated for example by Poole et al. (2016): “for monotonic nonlinearities $[\phi]$, this length map $[\mathcal{V}]$ is a monotonically increasing, concave function whose intersections with the unity line determine its fixed points.”

In this subsection, we build a *monotonic* activation function for which the \mathcal{V} map is not concave and admits an *infinite* number of stable fixed points.

Definition 1 (Activation function $\varphi_{\delta,\omega}$). For $\delta \in [0, 1]$ and $\omega > 0$ two real numbers, define:

$$\varphi_{\delta,\omega}(x) := x \exp\left(\frac{\delta}{\omega} \sin(\omega \ln |x|)\right). \quad (15)$$

It is easy to prove that for all $\delta \in [0, 1]$ and $\omega > 0$:

1. $\varphi_{\delta,\omega}(0) = 0$, by continuity;
2. $\varphi_{\delta,\omega}$ is odd;
3. $\varphi_{\delta,\omega}$ is strictly increasing;
4. the map¹⁰ $v \mapsto \int \varphi_{\delta,\omega}(\sqrt{v}z)^2 \mathcal{D}z$ is \mathcal{C}^1 and strictly increasing.

Definition 2 (Stable fixed points). Let $(u_n)_n$ be a sequence defined by recurrence:

$$u_{n+1} = f(u_n) \quad \text{with} \quad u_0 \in \mathbb{R}. \quad (16)$$

For any starting point a , we denote by $(u_n(a))_n$ the sequence defined as above, with $u_0 = a$.

We say that u^* is a stable fixed point of f if $f(u^*) = u^*$ and if there exists an open ball $\mathcal{B}(u^*, \epsilon)$ centered in u^* of radius $\epsilon > 0$ such that:

$$\forall a \in \mathcal{B}(u^*, \epsilon), \quad u_n(a) \xrightarrow{n \rightarrow \infty} u^*. \quad (17)$$

¹⁰Notation $\mathcal{D}z$ is defined in Eqn. (11).

Proposition 1. *If $f(u^*) = u^*$ and f is \mathcal{C}^1 in a neighborhood of u^* with $f'(u^*) \in (-1, 1)$, then u^* is a stable fixed point of f .*

Proposition 2. *For any $\delta \in (0, 1]$ and $\omega > 0$, let us use the activation function $\phi = \varphi_{\delta, \omega}$ of Definition 1. We consider the sequence $(v^l)_l$ defined by:*

$$\forall l \geq 0, \quad v^{l+1} = \sigma_w^2 \int \varphi_{\delta, \omega} \left(\sqrt{v^l} z \right)^2 \mathcal{D}z + \sigma_b^2, \quad \text{with } v^0 \in \mathbb{R}_*^+. \quad (18)$$

Then there exist $\sigma_w > 0$, $\sigma_b \geq 0$, and a strictly increasing sequence of stable fixed points $(v_k^)_{k \in \mathbb{Z}}$ of the recurrence equation (18).*

The proof can be found in Appendix A.1.

Remark 5. *In short, Proposition 2 ensures that there exists an infinite number of possible (nonzero) limits for the sequence $(v_a^l)_l$, depending on v_a^0 . Consequently, the proposed activation functions $\varphi_{\delta, \omega}$ are counterexamples to the claim of Poole et al. (2016).*

Plots. Figure 3 shows the shape of several activation functions $\varphi_{\delta, \omega}$ for various ω , along with their \mathcal{V} maps. We have chosen $\delta = 0.99 < 1$ to ensure that $\varphi_{\delta, \omega}$ is a strictly increasing function.¹¹ We have chosen $\sigma_b^2 = 0$ and $\sigma_w^2 = \sigma_\omega^2$, computed as indicated in Appendix A.2.

In Figure 3a, the proposed activation functions exhibit reasonable properties: they are non-linear, differentiable at each point (excluding 0), and remain dominated by a linear function. However, we expect that as ω grows, $\varphi_{\delta, \omega}$ should become closer and closer to the identity function,¹² which is not desirable for the activation function of a NN.

In Figure 3b, it is clear that the function $\varphi_{\delta, \omega}$ with $\omega = 6$ is a counterexample to the claim of Poole et al. (2016): two nonzero stable points appear. So, in that case, depending on the square norm v_a^0 of the input, the variance v_a^l of the pre-activations may converge to different values. For instance, for $\omega = 6$ and an input with square norm v_a^0 around the unstable point at $v \approx 2.3$, it may converge either to $v^* \approx 0.8$ or $v^* \approx 6.5$.

Also, we observe that for $\omega = 6$, the variance map \mathcal{V} tends to be closer to the identity function than for smaller ω . Thus, we expect the sequence $(v_a^l)_l$ to converge at a slower rate with $\omega = 6$ than with $\omega = 2$.

In Figure 3d, all the configurations lie in the chaotic phase. Since all the correlation maps \mathcal{C} are below the identity function, the sequence of correlations $(c_{ab}^l)_l$ always tends to 0. However, the plots are close to the identity, so $(c_{ab}^l)_l$ varies very slowly, and we expect that the correlation between data points propagates into the NN with little deformation. Despite being not perfect and lying in the chaotic phase, this configuration roughly preserves the input correlations between data points (without performing a pre-training phase), which is a desirable property at initialization: information propagates with little deformation to the output, and the error can be backpropagated to the first layers.

3.4 Maintaining a property of the pre-activations during propagation

To conclude this section and introduce the next one, we propose a common representation of the various methods used to build initialization distributions for the weights $(\mathbf{W}^l)_l$ and biases $(\mathbf{B}^l)_l$.

Several initialization methods (Glorot & Bengio, 2010, He et al., 2015, Poole et al., 2016, Schoenholz et al., 2017) are based on the same principle: initialization should be done in such a way that some characteristic κ^l of the distribution of \mathbf{Z}^l is preserved during propagation (e.g., $\kappa^l = \text{Var}(\mathbf{Z}^l)$). Intuitively, any change between κ^l and κ^{l+1} reflects a loss of information between \mathbf{Z}^l and \mathbf{Z}^{l+1} , which impacts propagation or backpropagation. For instance, when $\text{Var}(\mathbf{Z}^l) \rightarrow 0$, the network output tends to become deterministic, and when $\text{Var}(\mathbf{Z}^l) \rightarrow \infty$, the output tends to forget the operations made by the first layers (i.e., the gradients vanish during backpropagation).

¹¹We have chosen δ close to 1 to obtain a function $\varphi_{\delta, \omega}$ that is strongly nonlinear, but a bit lower than 1 to ensure that $\varphi'_{\delta, \omega}$ remains strictly positive, in order to prevent the training process from being stuck.

¹²As $\omega \rightarrow \infty$, $\varphi_{\delta, \omega}$ converges pointwise to the identity function.

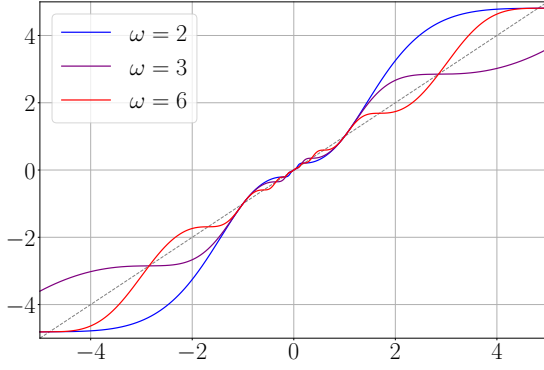
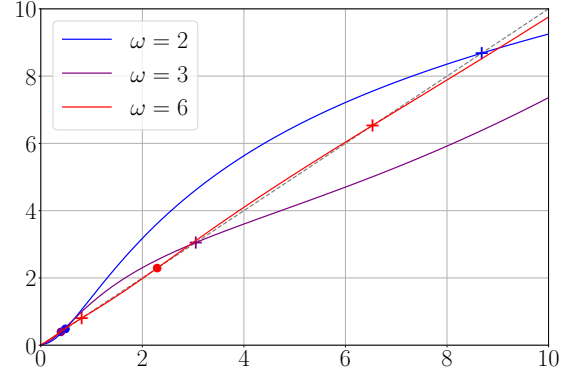
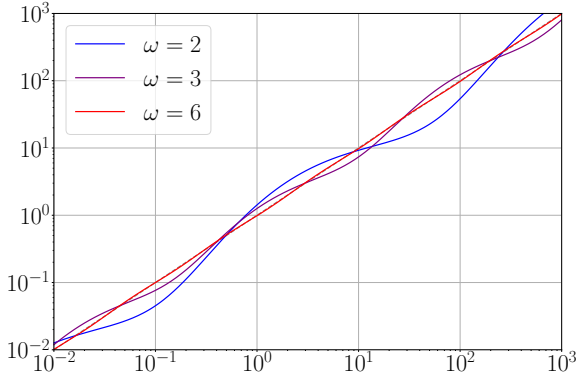
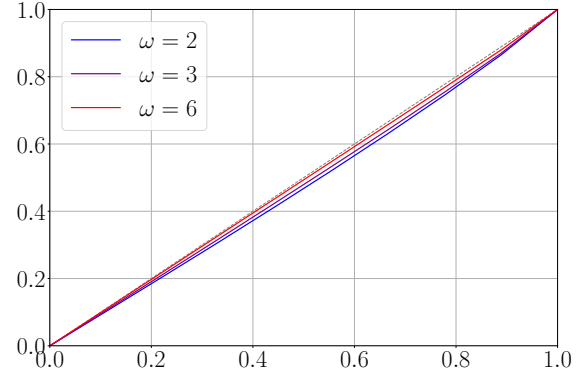
(a) Activation function $\varphi_{\delta, \omega}$.(b) Variance map $\mathcal{V}(\cdot | \sigma_w, \sigma_b = 0)$, linear scale.(c) Variance map $\mathcal{V}(\cdot | \sigma_w, \sigma_b = 0)$, log-log scale.(d) Correlation map $\mathcal{C}(\cdot, v^*, v^* | \sigma_w, \sigma_b)$.

Figure 3: Properties of the proposed counterexamples $\varphi_{\delta, \omega}$ represented in Fig. 3a for $\omega \in \{2, 3, 6\}$ and $\delta = 0.99$. Their variance map \mathcal{V} has an infinite number of fixed points.

In Fig. 3b, stable points are marked by crosses (+), and unstable points by bullets (•), when they are away from 0: two stable points appear for $\omega = 6$ (in red). As established in Proposition 2, σ_w is tuned for every ω in such a way that \mathcal{V} crosses the identity function an infinite number of times (not visible on the figure). In Fig. 3c (log-log scale), it is clearer that \mathcal{V} has an infinite number of fixed points, due to regular oscillations (in log-log scale) below and above the identity.

In Fig. 3d, we show that as ω grows, the correlation map \mathcal{C} becomes closer to the identity function, which means that the correlation between data points tends to propagate perfectly.

Note: since an infinite number of stable fixed points are available, we have arbitrarily picked one for each ω , denoted by v^* . This choice does not affect the plot of the correlation map \mathcal{C} , due to the very specific structure of $\varphi_{\delta, \omega}$.

More generally, we denote by \mathcal{D}^l the distribution associated to the pre-activations \mathbf{Z}^l , by $\mathcal{T}(\cdot; n_l, \mathbf{P}_l, \phi^l) =: \mathcal{T}_l[\mathbf{P}_l](\cdot)$ the transformation of \mathcal{D}^l performed by layer l , that is $\mathcal{D}^{l+1} = \mathcal{T}_l[\mathbf{P}_l](\mathcal{D}^l)$ (where \mathbf{P}_l is the initialization distribution of $(\mathbf{W}^l, \mathbf{B}^l)$ and ϕ^l is the activation function at layer l), and by $\kappa^l := \chi(\mathcal{D}^l)$ the characteristic of the distribution \mathcal{D}^l we are interested in. Then, according to a heuristic of “information preservation”, it is assumed that the sequence $(\kappa^l)_l$ must remain constant, and the initialization distributions $(\mathbf{P}_l)_l$ are built accordingly. In some cases, it is possible to build a map $\tilde{\mathcal{T}}_l[\mathbf{P}_l]$, so that each κ^{l+1} can be built out of its predecessor κ^l , without using all the information we may have on the $(\mathcal{D}^l)_l$.

We summarize this way of building initialization procedures in Figure 4, and we show how it applies to well-known initialization procedures in Table 1.

Table 1: Examples of \mathcal{D}^l , ϕ^l and χ in various setups. Notations: for any vector $\mathbf{x} \in \mathbb{R}^n$, its empirical mean is $\bar{\mathbb{E}} \mathbf{x} = \frac{1}{n} \sum_{i=1}^n x_i$ and its empirical variance is $\overline{\text{Var}} \mathbf{x} = \frac{1}{n-1} \sum_{i=1}^n (x_i - \bar{\mathbb{E}} \mathbf{x})^2$.

Method	\mathcal{D}^l	ϕ^l	χ	$\tilde{\mathcal{T}}_l[\mathbf{P}_l](\kappa)$	Assumption
Glorot & Bengio	distr. of \mathbf{Z}^l	Id	Var	$\sigma_w^2 \kappa^2 + \sigma_b^2$	–
He et al.	distr. of \mathbf{Z}^l	ReLU	Var	$\frac{1}{2} \sigma_w^2 \kappa^2 + \sigma_b^2$	–
Poole, Schoenholz	distr. of $(\mathbf{Z}_a^l, \mathbf{Z}_b^l)$	ϕ	corr	$\mathcal{C}_*(\kappa)$	$Z_{j;a}^l, Z_{j;b}^l$ Gaussian, $v_a^l = v_b^l = v^*$
Ours	distr. of \mathbf{Z}^l	$\phi_\theta^{\text{o/p}}$	Id	$\mathcal{T}_l[\mathbf{P}_l](\kappa)$	$\bar{\mathbb{E}} \mathbf{x}_a = \bar{\mathbb{E}} \mathbf{x}_b = 0,$ $\overline{\text{Var}} \mathbf{x}_a = \overline{\text{Var}} \mathbf{x}_b = 1$

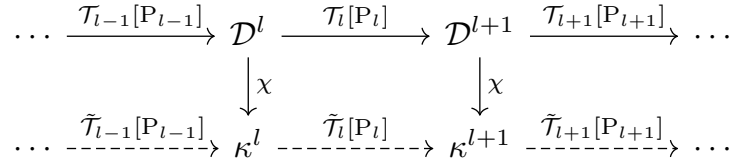


Figure 4: Building process of the initialization distributions \mathbf{P}_l of the parameters $(\mathbf{W}^l, \mathbf{B}^l)$: (i) the pre-activations-related distribution \mathcal{D}^l passes through a map $\mathcal{T}_l[\mathbf{P}_l]$ and becomes \mathcal{D}^{l+1} ; (ii) some statistical characteristic κ^l of \mathcal{D}^l can be computed with a function χ : $\kappa^l = \chi(\mathcal{D}^l)$; (iii) we tune the $(\mathbf{P}_l)_l$ in order to make the sequence $(\kappa^l)_l$ constant.

Remark 6. We can use Figure 4 to build new initialization distributions: first, we choose a statistical property of \mathbf{Z}^l , which determines \mathcal{D}^l and χ ; then, we build a framework in which $\chi(\mathcal{D}^l)$ can be easily computed for every l (e.g., we choose a specific activation function, or we make simplifying assumptions).

In the following section, we aim to impose Gaussian pre-activations through a specific activation function $\phi_\theta^{\text{o/p}}$ and initialization distribution \mathbf{P}_θ . It implies that we would preserve perfectly the distribution \mathcal{D}^l itself: our characteristic is $\chi(\mathcal{D}^l) = \mathcal{D}^l$. That way, *all the statistical properties of \mathcal{D}^l are preserved* during propagation.

4 Imposing Gaussian pre-activations

In this section, we propose a family of pairs $(\mathbf{P}_\theta, \phi_\theta^{\text{o/p}})$, where \mathbf{P}_θ is the distribution of the weights at initialization, $\phi_\theta^{\text{o/p}}$ is the activation function, and $\theta \in (2, \infty)$ is a parameter, such that the pre-activations Z_j^l are $\mathcal{N}(0, 1)$ at any layer l . Imposing such pre-activations is a way to meet two goals.

First, in Section 3.2, we have shown that the Gaussian hypothesis is not fulfilled in the case of realistic datasets propagated into a simple multilayer perceptron, and we have recalled in the Introduction that the tails of the pre-activations tend to become heavier when information propagates in a neural network. By

imposing Gaussian pre-activations, we ensure that the Gaussian hypothesis is true, which reconciles the results provided in the EOC setup (see Eqn. (9) and (10)) and the experiments.¹³

Second, as we recalled in the Introduction, many initialization procedures are based on the preservation of some characteristic of the distribution of the pre-activations (see Table 1 and Figure 4). Usual characteristics are the variance and the correlation between data points. By imposing Gaussian pre-activations, we would ensure that *the whole* distribution is propagated, and not only one of its characteristics.

Besides, we provide a set of constraints, Constraints 1, 2, 3, and 4, that the activation function and the initialization procedure should fulfill in order to maintain Gaussian pre-activations at each layer.

Summary. Formally, we aim to find a family of pairs $(P_\theta, \phi_\theta^{\text{o/p}})$ such that:

$$\left. \begin{array}{ll} Z_j^l \sim \mathcal{N}(0, 1) & \text{i.i.d.} \\ W_{ij}^l \sim P_\theta & \text{i.i.d.} \\ B_i^l = 0 \end{array} \right\} \Rightarrow Z_i^{l+1} := \frac{1}{\sqrt{n_l}} \mathbf{W}_i^l \phi_\theta^{\text{o/p}}(\mathbf{Z}^l) + \mathbf{B}^l \sim \mathcal{N}(0, 1),$$

where \mathbf{W}_i^l is the i -th row of the matrix \mathbf{W}^l . In other words, the pre-activations Z_i^{l+1} remain Gaussian for all l .

As a result of the present section, we make the following proposition for $(P_\theta, \phi_\theta^{\text{o/p}})$:

- P_θ is the symmetric Weibull distribution $\mathcal{W}(\theta, 1)$ with scale parameter 1 and shape (or tail) parameter θ , which is obtained by symmetrizing a standard Weibull distribution from \mathbb{R}^+ to \mathbb{R} (Generalized Weibull-Tail distributions are detailed in Definition 4). The symmetric Weibull distribution $\mathcal{W}(\theta, 1)$ has the following CDF:

$$F_W(t) = \frac{1}{2} + \frac{1}{2} \text{sgn}(t) \exp(-|t|^\theta); \quad (19)$$

- $\phi_\theta^{\text{o/p}}$ is computed to ensure that $Z_i^{l+1} := \frac{1}{\sqrt{n_l}} \mathbf{W}_i^l \phi_\theta^{\text{o/p}}(\mathbf{Z}^l) + \mathbf{B}^l$ is Gaussian $\mathcal{N}(0, 1)$. In short, the family of functions $\phi_\theta^{\text{o/p}}$ contains (Fig. 5):
 - a sub-family $(\phi_\theta^{\text{o}})_\theta$ of *odd* activation functions, spanning a range of functions from a tanh-like function (as $\theta \rightarrow 2^+$) to the identity function (as $\theta \rightarrow \infty$),
 - a sub-family $(\phi_\theta^{\text{p}})_\theta$ of *positive* activation functions, spanning a range of functions from a sigmoid-like function (as $\theta \rightarrow 2^+$) to a softplus-like function¹⁴ (as $\theta \rightarrow \infty$).

We shall see that ϕ_θ^{p} preserves the Gaussianity of pre-activations better than ϕ_θ^{o} .

In order to obtain this result, we:

1. reduce and decompose the initial problem (Section 4.1);
2. find constraints on the initialization distribution of the parameters to justify our choice $P_\theta = \mathcal{W}(\theta, 1)$ (Section 4.2);
3. compute the distribution Q_θ of $\phi_\theta^{\text{o/p}}(Z_j^l)$ we must choose to ensure Gaussian pre-activations Z_i^{l+1} , given an initialization distribution P_θ (Section 4.3);
4. build ϕ_θ^{o} and ϕ_θ^{p} from Q_θ (Section 4.4).

¹³There exists another way to solve this problem: use propagation equations which would take into account the sequence $(n_l)_l$ of layer widths, that is, adopt a non-asymptotic setup, contrary to the process leading to Eqn. (9) and (10). However, taking into account the whole sequence $(n_l)_l$ would lead to recurrence equations that are far less easy to use than Eqn. (12). Moreover, a precise characterization of the distributions $(\mathcal{D}^l)_l$ of the pre-activations $(Z_1^l)_l$ may be very difficult since they would not be Gaussian anymore.

¹⁴The softplus function is defined by: $x \mapsto \log(1 + \exp(x))$.

4.1 Decomposing the problem

By combining Equations (1) and (2), the operation performed by each layer is:

$$\mathbf{Z}^{l+1} = \frac{1}{\sqrt{n_l}} \mathbf{W}^l \phi(\mathbf{Z}^l) + \mathbf{B}^l. \quad (20)$$

In this subsection, we show that finding the distribution of the weights \mathbf{W}^l and the activation function ϕ in order to have:

$$\forall l \in [1, L], \forall j \in [1, n_l], \quad Z_j^l \sim \mathcal{N}(0, 1), \quad (21)$$

can be done if we manage to get:

$$Z := W\phi(X) \sim \mathcal{N}(0, 1), \quad \text{with } X \sim \mathcal{N}(0, 1), \quad (22)$$

by tuning the distribution of W and the activation function ϕ .

Z_i^{l+1} as a sum of Gaussian random variables. First, we focus on the operation made by one layer: if each layer transforms Gaussian inputs Z_j^l into pre-activations Z_i^{l+1} that are Gaussian too, then we can ensure that the pre-activations remain Gaussian after each layer. Thus, it is sufficient to solve the problem for one layer. After renaming the variables as $Z \leftarrow Z_i^{l+1}$, $W_j \leftarrow W_{ij}^l$, $X_j \leftarrow Z_j^l$, $B \leftarrow B_i^l$, $n \leftarrow n_l$, we have:

$$Z = \frac{1}{\sqrt{n}} \sum_{j=1}^n W_j \phi(X_j) + B. \quad (23)$$

In the rest of this subsection, we assume that the $X_j \sim \mathcal{N}(0, 1)$ are independent. We discuss the independence hypothesis in Remark 7 and Appendix B. We want to build an activation function ϕ , and distributions for $(W_j)_j$ and B such that $Z \sim \mathcal{N}(0, 1)$.

Second, we narrow our search space. According to Equation (23), Z is the sum of a random variable B and a number n of i.i.d. random variables $W_j \phi(X_j) / \sqrt{n}$. Since Z must be $\mathcal{N}(0, 1)$ whatever the value of n , it is both convenient and sufficient to check that each summand in the right-hand side of Equation (23) is Gaussian, that is:

$$B \sim \mathcal{N}(0, \sigma_b^2), \quad W_j \phi(X_j) \sim \mathcal{N}(0, 1 - \sigma_b^2), \quad (24)$$

with $\sigma_b \in (0, 1)$. In that case, we have $Z \sim \mathcal{N}(0, 1)$. For the sake of simplicity, we assume that $B = 0$ with probability 1, so that we just have to ensure that, for all j , $W_j \phi(X_j) \sim \mathcal{N}(0, 1)$. If one wants to deal with nonzero bias $B \sim \mathcal{N}(0, \sigma_b^2)$, it is sufficient to scale the random variables $W_j \phi(X_j)$ accordingly.

To summarize, we have chosen to build $Z \sim \mathcal{N}(0, 1)$ by ensuring that $W_j \phi(X_j) \sim \mathcal{N}(0, 1)$. With $B = 0$, this choice is formally imposed by this straightforward proposition.

Proposition 3 (Lévy-Cramér Theorem). *Let $(Z_j)_j$ be a sequence of n i.i.d. random variables. Let $Z = \frac{1}{\sqrt{n}} \sum_{j=1}^n Z_j$. If Z is $\mathcal{N}(0, 1)$, then the distribution of each Z_j is also $\mathcal{N}(0, 1)$.*

Proof. Let $\psi_Z(x) := \mathbb{E}[e^{iZx}]$ be the characteristic function of the distribution of Z . Besides, the $(Z_j)_j$ are i.i.d. and $Z = \frac{1}{\sqrt{n}} \sum_{j=1}^n Z_j$, so:

$$\psi_Z(x) = \exp\left(-\frac{x^2}{2}\right) \quad \text{and} \quad \psi_Z(x) = \left[\psi_{\frac{Z_1}{\sqrt{n}}}(x)\right]^n. \quad (25)$$

This proves that $\psi_{Z_1}(x) = e^{-x^2/2}$. So, for all j in $[1, n]$, $Z_j \sim \mathcal{N}(0, 1)$. □

As a result, we obtain the first constraint.

Constraint 1. *If, for all l , the weights $(W_{ij}^l)_{ij}$ are i.i.d. and independent from the pre-activations $(X_j^l)_j$, which are also supposed to be i.i.d., then we must ensure that:*

$$\forall l, i, j, \quad W_{ij}^l \phi(X_j^l) \sim \mathcal{N}(0, 1).$$

Remark 7. *The hypothesis of independent inputs $(X_j^l)_j$ truly holds only for the second layer.¹⁵ Although the hypothesis of independent $(X_j^l)_j$ is common (see Section 2), it is mostly unrealistic in practice. So, we propose in Appendix B an empirical study of this hypothesis, in order to identify in which cases the dependence between the inputs of one layer damages the Gaussianity of its outputted pre-activations.*

New formulation of the problem. We have proven that, to ensure that $Z \sim \mathcal{N}(0, 1)$, it is sufficient to solve the following problem:

$$\text{find } P \text{ and } \phi \text{ such that: } X \sim \mathcal{N}(0, 1) \text{ and } W \sim P \Rightarrow W\phi(X) \sim \mathcal{N}(0, 1). \quad (26)$$

In the following subsections, we build a family \mathcal{P} of initialization distributions (Section 4.2) such that, for any $P \in \mathcal{P}$, there exists a function ϕ such that (P, ϕ) is a solution to (26). We decompose the remaining problem into two parts, by introducing an intermediary random variable $Y = \phi(X)$:

- for a distribution P , deduce Q s.t.: $W \sim P, Y \sim Q \Rightarrow WY =: G \sim \mathcal{N}(0, 1)$ (Section 4.3);
- for a distribution Q , find a function ϕ s.t.: $X \sim \mathcal{N}(0, 1) \Rightarrow Y = \phi(X) \sim Q$ (Section 4.4).

4.2 Why initializing the weights W according to a symmetric Weibull distribution?

We are looking for a family \mathcal{P} of distributions such that, for any $P \in \mathcal{P}$, there exists Q such that:

$$W \sim P, Y \sim Q \Rightarrow WY =: G \sim \mathcal{N}(0, 1). \quad (27)$$

Therefore, the family \mathcal{P} is subject to several constraints. In this subsection, we present two results indicating that a subset of the family of Weibull distributions is a good choice for \mathcal{P} :

1. the density of W at 0 should be 0;
2. W should be a generalized Weibull-tail random variable (see Section 4.2.2 or Vladimirova et al., 2021) with parameter $\theta \in (2, \infty)$.

In the process, we are able to gather information about the distribution of $|Y|$, namely its density at 0 and the leading power of the log of its survival function at infinity, respectively:

$$f_{|Y|}(0) = \sqrt{\frac{2}{\pi}} \left[\int_0^\infty \frac{f_{|W|}(t)}{t} dt \right]^{-1}, \quad (28)$$

$$\log S_{|Y|}(y) \propto -y^{1/(\frac{1}{2} - \frac{1}{\theta})}. \quad (29)$$

As a conclusion of this subsection, we consider that the distribution $P = P_\theta$ of W should lie in the following subset of the family of symmetric Weibull distributions (defined at Eqn. (19)):

$$\begin{aligned} \mathcal{P} &:= \{\mathcal{W}(\theta, 1) : \theta \in \Theta\}, \\ \Theta &:= (2, \infty). \end{aligned}$$

¹⁵The inputs of the first layer are deterministic.

4.2.1 Behavior near 0

Since the product $G = WY$ is meant to be distributed according to $\mathcal{N}(0, 1)$, then we must have $f_{|G|}(0) = \sqrt{\frac{2}{\pi}} \in (0, \infty)$, which is impossible for several choices of distributions for W .

Proposition 4 (Density of a product of random variables at 0). *Let W, Y be two independent non-negative random variables and $Z = WY$. Let f_W, f_Y, f_Z be their respective densities. Assuming that f_Y is continuous at 0 with $f_Y(0) > 0$, we have:*

$$\text{if } \lim_{w \rightarrow 0} \int_w^\infty \frac{f_W(t)}{t} dt = \infty, \quad \text{then } \lim_{z \rightarrow 0} f_Z(z) = \infty. \quad (30)$$

Moreover, if f_Y is bounded:

$$\text{if } \int_0^\infty \frac{f_W(t)}{t} dt < \infty, \quad \text{then } f_Z(0) = f_Y(0) \int_0^\infty \frac{f_W(t)}{t} dt. \quad (31)$$

The proof can be found in Appendix C.

Corollary 1. *If f_Y and f_W are continuous at 0 with $f_Y(0) > 0$ and $f_W(0) > 0$, then:*

$$\lim_{z \rightarrow 0} f_Z(z) = \infty. \quad (32)$$

According to Corollary 1, it is impossible to obtain a Gaussian G by multiplying two random variables W and Y whose densities are both continuous and nonzero at 0. So, if we want to manipulate continuous densities, we must have either $f_W(0) = 0$ or $f_Y(0) = 0$.

Let us assume that $f_Y(0) = 0$. We want Y to be the image of $X \sim \mathcal{N}(0, 1)$ through the function ϕ , where $f_X(0) > 0$. So, in order to obtain Y with a zero density at 0, it is necessary to build a function ϕ with $\phi'(0) = \infty$ (see Lemma 2 in Appendix D), which is usually not desirable for an activation function of a neural network for training stability reasons.¹⁶ So, it is preferable to design W such that $f_W(0) = 0$.

Constraint 2. *To avoid activation functions with a vertical tangent at 0, the density of the initialization distribution of a weight W_{ij}^l must be 0 at 0:*

$$\forall l, i, j, \quad f_{W_{ij}^l}(0) = 0.$$

Remark 8. *In the common case of neural networks with activation function $\phi = \tanh$ and weights W initialized according to a Gaussian distribution, if we assume that the Gaussian hypothesis is true, then $f_Y(0) > 0$ and $f_Z(0) > 0$. Thus, Corollary 1 applies and the density of Z is infinite at 0.*

If $\phi = \text{Id}$, Z is the product of two independent $\mathcal{N}(0, 1)$, whose density is well-known:

$$f_Z(z) = \frac{K_0(|z|)}{\pi}, \quad (33)$$

where K_0 is the modified Bessel function of the second kind, which tends to infinity at 0, which illustrates Corollary 1.¹⁷

Finally, if Constraint 2 holds and we want $f_{|G|}(0) = \sqrt{\frac{2}{\pi}}$, then, according to Equation (31), the following constraint must hold.

¹⁶If $\phi'(0) = \infty$ and ϕ is \mathcal{C}^1 on \mathbb{R}^* , then numerical instabilities may occur during training: if a pre-activation Z_j^l approaches 0 too closely, $\phi'(Z_j^l)$ can explode and damage the training. These instabilities can be handled by gradient clipping (Pascanu et al., 2013).

¹⁷Though, even if each $W_j \phi(X_j)$ has an infinite density at 0, the density at 0 of the weighted sum $Z = \frac{1}{\sqrt{n}} \sum_{j=1}^n W_j \phi(X_j) + B$ may be finite. For instance, it occurs when all the W_j and $\phi(X_j)$ are i.i.d. and Gaussian. But in this case, even if $f_Z(0) < \infty$, it is impossible to recover a Gaussian pre-activation (see Prop. 3).

Constraint 3. *The density of Y at 0 must have a specific value depending on the distribution of W :*

$$f_{|Y|}(0) = \sqrt{\frac{2}{\pi}} \left[\int_0^\infty \frac{f_{|W|}(t)}{t} dt \right]^{-1}.$$

4.2.2 Behavior of the tail

We use the results of [Vladimirova et al. \(2021\)](#) on the *generalized Weibull-tail distributions* and start by recalling useful definitions and properties.

Definition 3 (Slowly varying function). *A measurable function $f : (0, \infty) \rightarrow (0, \infty)$ is said to be slowly varying if:*

$$\forall a > 0, \quad \lim_{x \rightarrow \infty} \frac{f(ax)}{f(x)} = 1. \quad (34)$$

Definition 4 (Generalized Weibull-Tail (GWT) distribution, [Vladimirova et al., 2021](#)). *A random variable X is called generalized Weibull-tail with parameter $\theta > 0$, or $\text{GWT}(\theta)$, if its survival function S_X is bounded in the following way:*

$$\forall x > 0, \quad \exp(-x^\theta f_1(x)) \leq S_X(x) \leq \exp(-x^\theta f_2(x)), \quad (35)$$

where f_1 and f_2 are slowly-varying functions and $\theta > 0$.

Proposition 5 ([Vladimirova et al., 2021](#), Thm. 2.2). *The product of two independent non-negative random variables $|W|$ and $|Y|$ which are respectively $\text{GWT}(\theta_W)$ and $\text{GWT}(\theta_Y)$ is $\text{GWT}(\theta)$, with θ such that:*

$$\frac{1}{\theta} = \frac{1}{\theta_W} + \frac{1}{\theta_Y}. \quad (36)$$

We recall that, in our case, $|G| = |W| \cdot |Y|$ is the absolute value of a Gaussian random variable. So $|G|$ is $\text{GWT}(2)$. Thus, if we assume that $|W|$ and $|Y|$ are respectively $\text{GWT}(\theta_W)$ and $\text{GWT}(\theta_Y)$, then we have:

$$\frac{1}{2} = \frac{1}{\theta_W} + \frac{1}{\theta_Y}. \quad (37)$$

Therefore we have the following constraint.

Constraint 4. *The weights W are $\text{GWT}(\theta)$ with $\theta \in \Theta = (2, \infty)$.*

4.2.3 Conclusion

Constraints 2 and 4 indicate that the distribution P of the weights W :

- (i) should have a density f_W such that $f_W(0) = 0$;
- (ii) should be $\text{GWT}(\theta)$ with $\theta \in (2, \infty)$.

A simple choice for P matching these two conditions is: $P = P_\theta = \mathcal{W}(\theta, 1)$ with $\theta \in (2, \infty)$, where $\mathcal{W}(\theta, 1)$ is the symmetric Weibull distribution, defined in Equation (19). Thus, we ensure that $f_W(0) = 0$ and W is generalized Weibull-tail with a parameter θ easy to control (see remark below).

Remark 9. *If $W \sim \mathcal{W}(\theta, 1)$, then W is $\text{GWT}(\theta)$.*

4.3 Obtaining the distribution of the activations Y

Now that the distribution P of W is supposed to be symmetric Weibull, that is, $P = P_\theta = \mathcal{W}(\theta, 1)$, we are able to look for *odd* and *positive* activation functions $\phi_\theta^{\text{o/p}}$ such that:

$$W \sim \mathcal{W}(\theta, 1), X \sim \mathcal{N}(0, 1) \Rightarrow W\phi_\theta^{\text{o/p}}(X) \sim \mathcal{N}(0, 1). \quad (38)$$

As a first step, we look for a distribution Q_θ such that:

$$W \sim P_\theta, Y \sim Q_\theta \Rightarrow WY =: G \sim \mathcal{N}(0, 1). \quad (39)$$

In order to “invert” this equation, it is natural to make use of the Mellin transform. A comprehensive and historical work about Fourier and Mellin transforms can be found in [Titchmarsh \(1937\)](#), and a simple application to the computation of the density of the product of two random variables can be found in [Epstein \(1948\)](#).

However, the technique involving the Mellin transform is very difficult to use in this case, both analytically and numerically. Details about the Mellin transform and these difficulties can be found in [Appendix E](#).

Computation of $f_{|Y|}$: hand-designed parameterized function. Thus, inspired by the shape of $f_{|Y|}$ computed via the numerical inverse Mellin transform (see [Fig. 13](#), [App. E.2](#)), we build an approximation of $f_{|Y|}$ from the family of functions $\{g_{\alpha, \gamma, \lambda_1, \lambda_2} : \alpha, \gamma, \lambda_1, \lambda_2 > 0\}$ with:

$$g_\Lambda(x) := g_{\alpha, \gamma, \lambda_1, \lambda_2}(x) := \gamma \alpha \frac{x^{\alpha-1}}{\lambda_1^\alpha} \exp\left(-\frac{x^\alpha}{\lambda_1^\alpha}\right) + \sqrt{\frac{2}{\pi}} \frac{1}{\Gamma(1 - \frac{1}{\theta})} \exp\left(-\frac{x^{\theta'}}{\lambda_2^{\theta'}}\right), \quad (40)$$

where θ' is the conjugate of θ : $\frac{1}{\theta} + \frac{1}{\theta'} = \frac{1}{2}$, and $\Lambda := (\alpha, \gamma, \lambda_1, \lambda_2)$. It is clear that, whatever the parameters, $g_\Lambda(0) = \sqrt{\frac{2}{\pi}} [\Gamma(1 - \frac{1}{\theta})]^{-1}$, which is exactly [Constraint 3](#). Moreover, when $\alpha = 0$, g matches also [Constraint 4](#).

Then, we optimize the vector of parameters Λ with respect to the following loss:

$$\ell(\Lambda) := \|\hat{F}_\Lambda - F_{|G|}\|_\infty \quad (41)$$

$$\hat{F}_\Lambda(z) := \int_0^\infty F_{|W|}\left(\frac{z}{t}\right) g_\Lambda(t) dt \quad (\text{see Eqn. (57)}), \quad (42)$$

where \hat{F}_Λ is meant to approximate the CDF of the absolute value of a Gaussian $\mathcal{N}(0, 1)$. The integral is computed numerically. For the loss, we have chosen to compute the \mathcal{L}^∞ -distance between two CDFs, in order to be consistent with the Kolmogorov–Smirnov test we perform in [Section 5.1](#). Optimization details can be found in [Appendix F](#).

4.4 Obtaining the activation function $\phi_\theta^{\text{o/p}}$

In the preceding section, we have computed the distribution of $|Y|$. We are restricting ourselves to respectively symmetrical and positive Y , whose distributions are respectively denoted by Q_θ^{o} and Q_θ^{p} (“o” for “odd” and “p” for “positive”). Now, we want to build the activation function $\phi_\theta^{\text{o/p}}$, in order to transform a pre-activation $G \sim \mathcal{N}(0, 1)$ into an activation $Y = \phi_\theta^{\text{o/p}}(G)$ distributed according to $Q_\theta^{\text{o/p}}$:

$$\text{if } G \sim \mathcal{N}(0, 1), \quad \text{then } \phi_\theta^{\text{o/p}}(G) \sim Q_\theta^{\text{o/p}}.$$

To compute $\phi_\theta^{\text{o/p}}$, we will use the following proposition:

Proposition 6. *Let X be a random variable such that F_X is strictly increasing on \mathbb{R} . Let Q be a distribution without atoms such that F_Q is strictly increasing on $S := F_Q^{-1}((0, 1))$. Then:*

$$\text{with } \phi(x) := F_Q^{-1}(F_X(x)), \quad \text{we have: } \phi(X) \sim Q. \quad (43)$$

Proof. Let $\phi(x) := F_Q^{-1}(F_X(x))$, which is a strictly increasing bijection from \mathbb{R} to S .

For any $y \in S$, we have:

$$\mathbb{P}(\phi(X) \leq y) = \mathbb{P}(X \leq \phi^{-1}(y)) = F_X(\phi^{-1}(y)) = F_X(F_X^{-1}(F_Q(y))) = F_Q(y). \quad (44)$$

For $y \notin S$, since S is connected, we have either $y \leq \inf S$ or $y \geq \sup S$:

- if $y \notin S$ with $y \leq \inf S$, then $\mathbb{P}(\phi(X) \leq y) \leq \mathbb{P}(\phi(X) \notin S) = 0$;
- if $y \notin S$ with $y \geq \sup S$, then $\mathbb{P}(\phi(X) \leq y) \geq \mathbb{P}(\phi(X) \leq \sup S) \geq \mathbb{P}(\phi(X) \in S) = 1$.

So, for all $y \in \mathbb{R}$, $\mathbb{P}(\phi(X) \leq y) = F_Q(y)$. □

Odd activation function ϕ_θ^o . We build a symmetric distribution for Y :

$$F_Y^o(t) := \frac{1}{2} + \frac{1}{2} \text{sgn}(t) \int_0^{|t|} f_{|Y|}(y) dy. \quad (45)$$

Since F_G and F_Y^o are strictly increasing on \mathbb{R} , we can use Proposition 6:

$$\phi_\theta^o(t) := (F_Y^o)^{-1}(F_G(t)). \quad (46)$$

Positive activation function ϕ_θ^p . We build a distribution for Y with support in \mathbb{R}^+ :

$$F_Y^p(t) := \int_0^{\max(0,t)} f_{|Y|}(y) dy. \quad (47)$$

Since F_G is strictly increasing on \mathbb{R} and F_Y^p is strictly increasing on $S := (F_Y^p)^{-1}((0,1)) = \mathbb{R}^+ \setminus \{0\}$, we can use Proposition 6:

$$\phi_\theta^p(t) := (F_Y^p)^{-1}(F_G(t)). \quad (48)$$

Remark 10. *There are many other possible choices for the distribution Q of Y , resulting in various activation functions other than $\phi_\theta^{o/p}$. However, among all the possible distributions Q , we identify two “natural” usable solutions: Q symmetric (leading to an odd activation function) or Q with support in \mathbb{R}^+ (leading to a positive activation function).*

4.5 Results and limiting cases

We have plotted in Figure 5 the different distributions related to the computation of $\phi_\theta^{o/p}$ and the functions $\phi_\theta^{o/p}$ themselves. The family of the ϕ_θ^o is a continuum spanning unbounded functions from the tanh-like function ϕ_{2+} to the identity function, while the family of the ϕ_θ^p is a continuum spanning functions from a sigmoid-like function to a softplus-like function, all of which tending to 0 in $-\infty$ and to $+\infty$ in $+\infty$. As a reminder, $\text{softplus}(x) = \log(1 + \exp(x))$.

Our construction degenerates into the following two extreme cases at the boundaries of the parameter space $\Theta = (2, \infty)$:

- when $\theta \rightarrow \infty$, we have $P_\theta \xrightarrow{d} \mathcal{R}$ and:
 - $\phi_\theta^o \rightarrow \text{Id}$ pointwise,
 - $\phi_\theta^p \rightarrow \phi_\infty^p$ pointwise, with: $\phi_\infty^p : x \mapsto \sqrt{2} \text{erf}^{-1}(\frac{1}{2} + \frac{1}{2} \text{erf}(\frac{x}{\sqrt{2}}))$;
- when $\theta \rightarrow 2$, we have $P_\theta \xrightarrow{d} \mathcal{W}(2, 1)$;

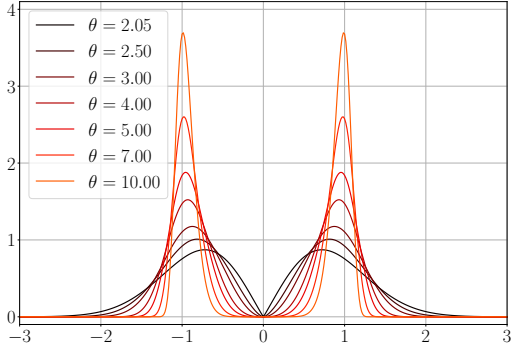
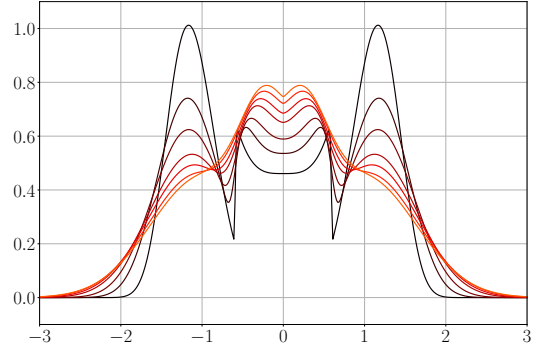
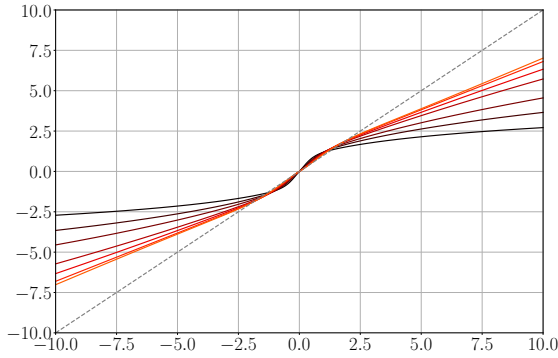
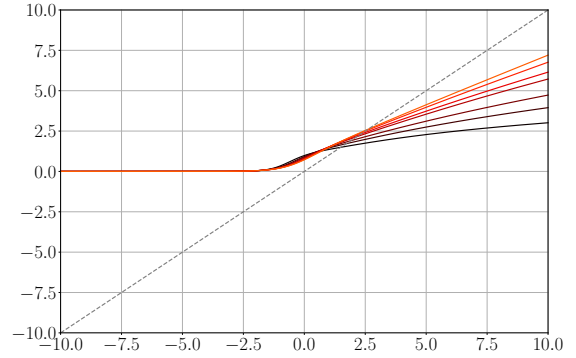
(a) Initialization distribution P_θ of the weights: symmetric Weibull $\mathcal{W}(\theta, 1)$.(b) Estimated density f_Y of the distribution Q_θ of Y .(c) Activation function ϕ_θ^o .(d) Activation function ϕ_θ^p .

Figure 5: How to build a random variable $WY = W\phi_\theta^{o/p}(X) =: G \sim \mathcal{N}(0, 1)$, where $X \sim \mathcal{N}(0, 1)$? (a) Choose the distribution P_θ of W , then (b) deduce the distribution Q_θ of Y , and finally (c-d) find ϕ_θ^o and ϕ_θ^p .

where \mathcal{R} is the Rademacher distribution ($\xi \sim \mathcal{R} \Leftrightarrow \mathbb{P}(\xi = \pm 1) = \frac{1}{2}$) and Id is the identity function.

In the limiting case $\theta \rightarrow \infty$, we initialize the weights at ± 1 , which corresponds to binary “weight quantization”, used in neural networks compression (Pouransari et al., 2020), and we use a linear activation function, commonly used in theoretical analyses of neural networks (Arora et al., 2019a). In the limiting case $\theta \rightarrow 2$, we recover weights with Gaussian tails, with a tanh-like or sigmoid-like activation function.

5 Experiments

In this section, we test the Gaussian hypothesis with ReLU, tanh and our activation functions $\phi_\theta^{o/p}$, after one layer (Section 5.1) and after several layers (Section 5.2). Then, we plot the Edge of Chaos graphs (σ_b, σ_w), which are exact with $\phi = \phi_\theta^{o/p}$ (Section 5.3) in the case of finite n_l with independent pre-activations. Finally, in Section 5.4, we show the training trajectories of LeNet-type networks and multilayer perceptrons, when using tanh, ReLU, and various activation functions we have proposed.

In the following subsections, when we use $\phi = \tanh$ or ReLU, we initialize the weights according to a Gaussian at the EOC. This is, for tanh: $\sigma_b^2 = 0.013$, $\sigma_w^2 = 1.46$; and for ReLU: $\sigma_b^2 = 0$, $\sigma_w^2 = 2$. When we use $\phi = \phi_\theta^{o/p}$, we initialize the weights according to $\mathcal{W}(\theta, 1)$.

Notation for the activation functions. We recall that: ϕ denotes an arbitrary activation function; $\varphi_{\delta,\omega}$ denotes the function defined in Definition 1; $\phi_{\theta}^{\text{o/p}}$ denotes the odd or the positive function verifying Eqn. (38).

5.1 Testing the Gaussian hypothesis: synthetic data, one layer

Most importantly, we must experimentally verify that our family of initialization distributions and activation functions $\{(P_{\theta}, \phi_{\theta}^{\text{o/p}}) : \theta \in (2, \infty)\}$ can reliably produce Gaussian pre-activations.

Framework. First, we test our setup in the one-layer neural network case with synthetic inputs. More formally, we consider a $\mathcal{N}(0, 1)$ *pre-input*¹⁸ $\mathbf{Z} \in \mathbb{R}^n$, which is meant to be first transformed by the activation function $\phi_{\theta}^{\text{o/p}}$ (hence the name “pre-input”), then multiplied by a matrix of weights $\mathbf{W} \in \mathbb{R}^{1 \times n}$. This one-neuron layer outputs a scalar Z' :

$$Z' := \frac{1}{\sqrt{n}} \mathbf{W} \phi(\mathbf{Z}), \quad \text{with } Z_j \sim \mathcal{N}(0, 1) \text{ and } W_{1j} \sim P_{\theta} \text{ for all } j. \quad (49)$$

We want to check that the distribution P' of Z' is equal to $\mathcal{N}(0, 1)$.

Experimental results. For that, we use of the Kolmogorov–Smirnov (KS) test (Kolmogoroff, 1941, Smirnov, 1948) (see Appendix G). We perform the KS test within two setups: with and without preliminary standardization of the sets of samples. With a preliminary standardization, we perform the test on $(\bar{Z}'_1, \dots, \bar{Z}'_s)$:

$$\bar{Z}'_k = \frac{Z'_k - \bar{\mu}}{\bar{\sigma}}, \quad \bar{\mu} = \frac{1}{s} \sum_{k=1}^s Z'_k, \quad \bar{\sigma}^2 = \frac{1}{s-1} \sum_{k=1}^s (Z'_k - \bar{\mu})^2. \quad (50)$$

For the sake of simplicity, let us denote by $\hat{F}_{Z'} := F_s$ the empirical CDF of Z' , computed with the s data samples (Z'_1, \dots, Z'_s) , and let $\hat{F}_{\bar{Z}'}$ be the empirical CDF of standardized Z' , computed with $(\bar{Z}'_1, \dots, \bar{Z}'_s)$.

We have plotted in Figure 6 the KS statistic of the distribution of the output Z' , when using our activation functions $\phi_{\theta}^{\text{o/p}}$, tanh and ReLU. Our sample size is $s = 10^7$. A small KS statistic corresponds to a configuration where Z' is close to being $\mathcal{N}(0, 1)$. If a point is above the KS threshold (green line, dotted), then the Gaussian hypothesis is rejected with p -value 0.05.

When we perform standardization (Fig. 6b), the neurons using $\phi_{\theta}^{\text{o/p}}$ output always a pre-activation Z' that is closer to $\mathcal{N}(0, 1)$ than with ReLU or tanh. But, despite this advantage, the Gaussian hypothesis should be rejected with $\phi_{\theta}^{\text{o/p}}$ when the neuron has a very small number of inputs ($n < 30$).

In Figure 6a, we compare directly the distribution of Z' to $\mathcal{N}(0, 1)$. This test is harder than testing the Gaussian hypothesis because the variance of Z' must be equal to 1. We observe that when using $\phi_{\theta}^{\text{o/p}}$, the KS statistic remains above the threshold (while it is still below 10^{-2} , and even below $6 \cdot 10^{-3}$ for $n \geq 3$). This result is due to the fact that our computation of $\phi_{\theta}^{\text{o/p}}$ is only approximate (see Section 4.4).

Remark 11. Our sample size ($s = 10^7$) is very large, which lowers the threshold of rejection of the Gaussian hypothesis. We have chosen this large s to reduce the noise of the KS statistics. If we had chosen $s = 18000$, a threshold close to 10^{-2} would have resulted, which is higher than any of the KS statistics computed with $\phi = \phi_{\theta}^{\text{o/p}}$. One will also note that, in Section 5.2, we use only $s = 10000$ samples to keep a reasonable computational cost.

Remark 12. Since tanh and ReLU have not been designed such that $Z' \sim \mathcal{N}(0, 1)$, we did not plot the related non-standardized KS statistics in Figure 6a. Anyway, given the standard deviation of Z' when using $\phi = \tanh$ or ReLU (see Table 2, Appendix H.3), very large KS statistics are expected in this setup.

We discuss the limits of the KS test in Appendix G.

¹⁸Such a pre-input plays the role of the pre-activation outputted by a hypothetical preceding layer.

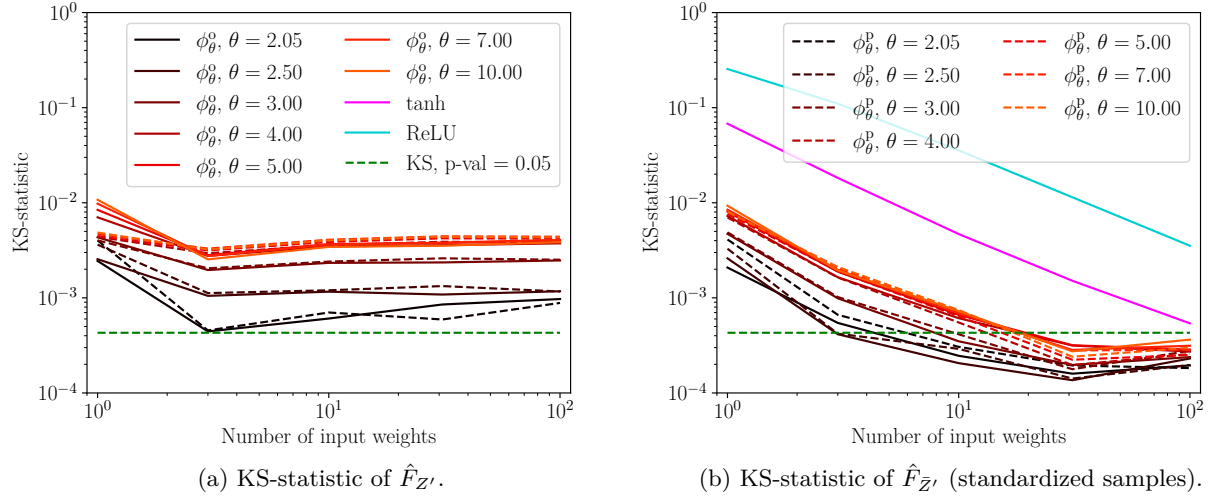


Figure 6: Evolution of the KS statistic of the distribution of Z' (Fig. 6a) and the standardized distribution of Z' (Fig. 6b), with a number of inputs $n \in \{1, 3, 10, 30, 100\}$.

5.2 Testing the Gaussian hypothesis: CIFAR-10, multilayer perceptron

Now, we test our setup on a multilayer perceptron with CIFAR-10, which is more realistic. We show in Figure 7 how the distribution of the pre-activations propagates in a multilayer perceptron, for different layer widths $n_l \in \{10, 100, 1000\}$.

Setup. Let \mathcal{D}^l be the distribution of the pre-activation Z_1^l after layer l . For all l , let us define $(Z_{1;k}^l)_{k \in [1,s]}$, a sequence of i.i.d. samples drawn from \mathcal{D}^l . The plots in Figure 7 show the evolution of the \mathcal{L}^∞ distance $\|\hat{F}_{Z_1^l} - F_G\|_\infty$ between the CDF of $\mathcal{N}(0, 1)$, F_G , and the empirical CDF of \mathcal{D}^l , $\hat{F}_{Z_1^l}$, built with $s = 10000$ samples $(Z_{1;k}^l)_{k \in [1,s]}$.

We have built the plots of Figure 7 with the same input data point.¹⁹ See Appendix H.4 for a comparison of the propagation between different data points. Also, the propagated data point has been normalized according to the whole training dataset, that is:

Definition 5 (Input normalization over the whole dataset). *We build the normalized data point $\hat{\mathbf{x}}$:*

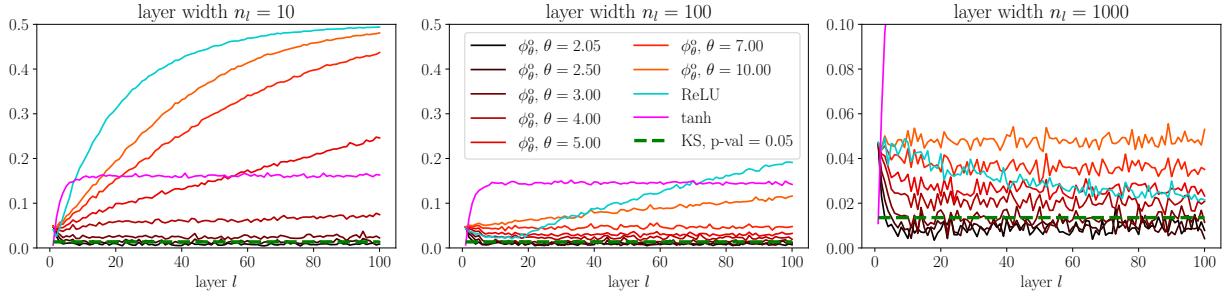
$$\hat{x}_{a;ij} := \frac{x_{a;ij} - \mu_i}{\sigma_i}, \quad \mu_i := \frac{1}{p_i d} \sum_{\mathbf{x} \in \mathbb{D}} \sum_{j=1}^{p_i} x_{ij}, \quad \sigma_i^2 := \frac{1}{p_i d - 1} \sum_{\mathbf{x} \in \mathbb{D}} \sum_{j=1}^{p_i} (x_{ij} - \mu_i)^2, \quad (51)$$

where $x_{a;ij}$ is the j -th component of the i -th channel of the input image \mathbf{x}_a , p_i is the size of the i -th channel, and d is the size of the dataset \mathbb{D} .

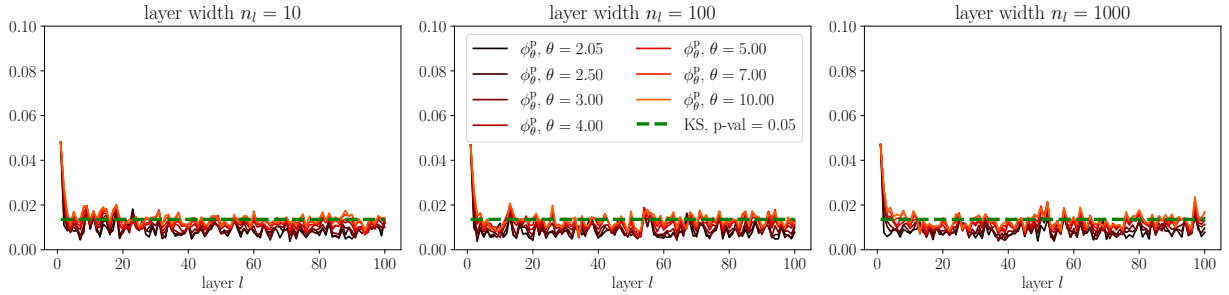
Results. First, in all cases, \tanh leads to pre-activations that remain far from the standard Gaussian. Also, with 10 and 100 neurons per layer and ReLU , the pre-activations tend to diverge from the standard Gaussian.

Second, our proposition of activation functions $\phi = \phi_\theta^{o/p}$ leads to various results, depending on the layer width n_l and the subfamily to which it belongs, $(\phi_\theta^o)_\theta$ or $(\phi_\theta^p)_\theta$. On one hand, the positive activation functions ϕ_θ^p lead consistently to standard Gaussian pre-activations for all $\theta \in [2.05, 10]$ (Fig. 7b). On the other hand, the odd activation functions ϕ_θ^o lead consistently to Gaussian pre-activations only for small θ (Fig. 7a).

¹⁹In the PyTorch implementation of the training set of CIFAR-10: data point #47981 (class = plane). This data point has been chosen randomly.



(a) Distance $\|\hat{F}_{Z_1^l} - F_G\|_\infty$; odd activation function ϕ_θ^o ; inputs normalized over the dataset (Definition 5).



(b) Distance $\|\hat{F}_{Z_1^l} - F_G\|_\infty$; positive activation function ϕ_θ^p ; inputs normalized over the dataset (Definition 5); **these figures have been zoomed around 0.**

Figure 7: Evolution of the distance between \mathcal{D}^l and the standard Gaussian, during propagation where l varies from 1 to 100. If the pre-activations are Gaussian, these curves should remain close to zero. The dotted green line is the KS threshold: any point above it corresponds to a distribution \mathcal{D}^l for which the Gaussian hypothesis should be rejected with p -value 0.05. Weight initialization is $\mathcal{W}(\theta, 1)$ when using $\phi = \phi_\theta^{o/p}$ and is Gaussian according to the EOC when using $\phi = \tanh$ or ReLU.

Conclusion. For all tested widths, combining a positive activation function ϕ_θ^p and weights sampled from $\mathcal{W}(\theta, 1)$ leads to pre-activations that are close to $\mathcal{N}(0, 1)$, and obviously closer to $\mathcal{N}(0, 1)$ than with tanh or ReLU. However, our proposition of odd activation functions ϕ_θ^o leads to a distribution of pre-activations that drifts away from $\mathcal{N}(0, 1)$ along the propagation, at least for $\theta > 2.5$. These results are confirmed with various inputs, as shown in Figures 16 and 17 in Appendix H.4.

So, in the case $\phi = \phi_\theta^p$, $\mathcal{D}^l = \mathcal{N}(0, 1)$ is close to a stable fixed point of the recurrence relation $\mathcal{D}^{l+1} = \mathcal{T}_l[\mathbf{P}_l](\mathcal{D}^l)$ with the notations of Section 3.4 (see Fig. 4). But, in the case $\phi = \phi_\theta^o$, $\mathcal{D}^l = \mathcal{N}(0, 1)$ is not a stable fixed point. This deviation from the expected result is likely to be due to the assumption of independent pre-activations, which we used in the derivation of both ϕ^o and ϕ^p . This assumption is discussed in Appendix B, where we show that such dependence plays a more important role with ϕ^o than with ϕ^p .

This search for stable fixed points in the recurrence relation $\mathcal{D}^{l+1} = \mathcal{T}_l[\mathbf{P}_l](\mathcal{D}^l)$ is closely related to the discovery of stable fixed points for the sequence of variances $(v_a^l)_l$ and the sequence of correlations $(c_{ab}^l)_l$ (Poole et al., 2016, Schoenholz et al., 2017), and may be explored further in future works.²⁰

5.3 Non-asymptotic Edge of Chaos

In Figure 8, we show the Edge of Chaos graphs for several activation functions: tanh and ReLU on one side, and our family $(\phi_\theta^{o/p})_\theta$ on the other side. We remind that each graph corresponds to a family of initialization standard deviations (σ_w, σ_b) such that the sequence of correlations $(c_{ab}^l)_l$ converges to 1 at a *sub-exponential* rate (see Section 3.1, Point 2). Such choices ensure that the initial correlation between two inputs changes slowly so that the information contained in these inputs is lost at the slowest possible rate.

Instead of assuming that the pre-activations are Gaussian as an effect of the “infinite-width limit” and the Central Limit Theorem, we claim that, with our activation functions ϕ_θ^o , for any layer widths (including narrow layers and networks with various layer widths), the Edge of Chaos is *non-asymptotic*. Therefore, the corresponding curves in Figure 8 hold for realistic networks.

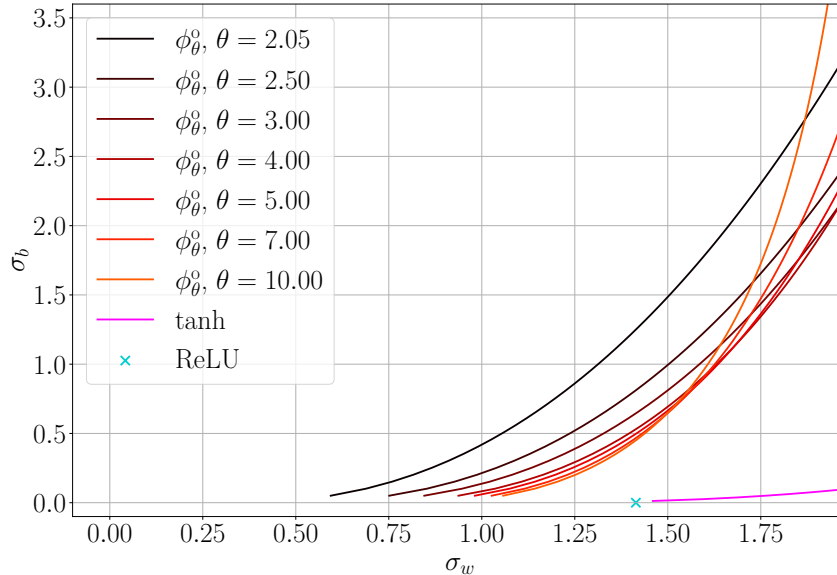


Figure 8: Edge of Chaos for several activation functions. The ordered phase (resp. chaotic) lies above (resp. below) each EOC curve.

²⁰The fixed points of $\mathcal{D}^{l+1} = \mathcal{T}_l[\mathbf{P}_l](\mathcal{D}^l)$ can also be seen as stationary distributions of the Markov chain $(Z_1^l)_l$, if the layer width n_l and the initialization distribution \mathbf{P}_l are constant.

Remark 13. For the ReLU activation function, the EOC graph reduces to one point. One can refer to [Hayou et al. \(2019, Section 3.1\)](#) for a complete study of the EOC of “ReLU-like functions”, that is, functions that are linear on \mathbb{R}^+ and on \mathbb{R}^- with possibly different factors.

Also, as in Figure 1 (see Section 3.2), we have plotted the propagation of the correlations $(C_{pq}^l)_l$ with $\phi = \phi_\theta^o$ and weights sampled from $\mathcal{W}(\theta, 1)$ in Appendix H.2.

5.4 Training experiments

Finally, we compare the performance of a trained neural network when using tanh and ReLU, and our activation functions. Although the EOC framework (and ours) do not provide any quantitative prediction about the training trajectories, it is necessary to analyze them in order to enrich the theory.

This section starts with a basic check of the training and test performances on a common task: training LeNet on CIFAR-10. Then, we challenge our activation function, along with tanh and ReLU, by training on MNIST a diverse set of multilayer perceptrons, some of them being extreme (narrow and deep).

In the following, we train all the neural networks with the same optimizer, Adam, and the same learning rate $\eta = 0.001$. We use a scheduler and an early stopping mechanism, respectively based on the training loss and the validation loss, the test loss not being used during training. We did not use data augmentation. All the technical details are provided in Appendix H.5.

LeNet-type networks. We provide here the results only for our odd activation functions ϕ_θ^o . The results with the positive ones ϕ_θ^p are provided in Appendix H.6. The results are very similar in both cases.

We consider LeNet-type networks (LeCun et al., 1998). They are made of two (5×5) -convolutional layers, each of them followed by a 2-stride average pooling, and then three fully-connected layers. We denote by “6 – 16 – 120 – 84 – 10” a LeNet neural network with two convolutional layers outputting respectively 6 and 16 channels, and three fully connected layers having respectively 120, 84, and 10 outputs (the final output of size 10 is the output of the network).

We have tested LeNet with several sizes (see Figure 9). In Figure 9a, we have plotted the training loss. Overall, ReLU and tanh perform well, along with some ϕ_θ^o with small θ and $\varphi_{\delta, \omega}$, with $(\delta, \omega) = (0.99, 2)$. In Figure 9b, the results in terms of test accuracy are quite different: ReLU and tanh still achieve good accuracy, but the other functions achieving similar results on the training loss seem to be a bit behind.

So, in this standard setup, the functions we are proposing seem to make the neural network trainable and as expressive as with other activation functions, but with some overfitting. This is not surprising, since we are testing long-standing activation functions, ReLU and tanh, which have been selected both for their ability to make the neural network converge quickly with good generalization, against functions we have designed only according to their ability to propagate information. Therefore, according to these plots, taking into account generalization may be the missing piece of our study.

Multilayer perceptron. We provide here the results only for our odd activation functions ϕ_θ^o . The results with the positive ones ϕ_θ^p are provided in Appendix H.6. The results are very different compared to the previous experiment: training narrow and deep neural networks is much more difficult with the positive activation functions than with the odd ones.

We have trained a family of multilayer perceptrons on MNIST. They have a constant width $n_l \in \{3, 10\}$ and a depth $L \in \{3, 10, 30\}$. So, extreme cases such as a narrow and deep neural network ($n_l = 3$, $L = 30$) have been tested.

A series of results are presented in Figure 10. The training curves have been averaged over 5 experiments. In terms of training, the strength of our activation functions ϕ_θ is more visible in the case of narrow neural networks ($n_l = 3$): in general, the loss decreases faster and attains better optima with $\phi = \phi_\theta$ than with $\phi = \tanh$ or ReLU.

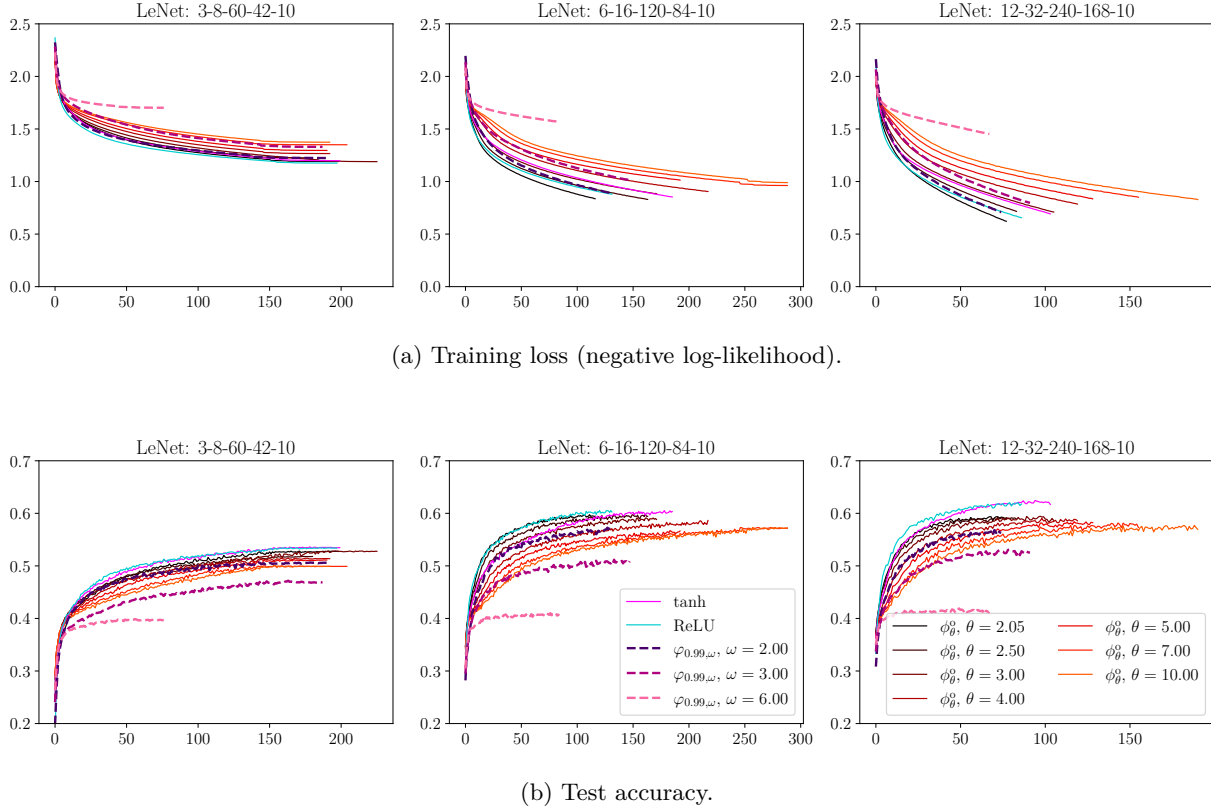


Figure 9: Training curves for LeNet with 3 different numbers of neurons per layer.

We also notice that training a narrow and deep neural network with a ReLU activation function is challenging. This result is consistent with several observations we have made in Section 3.2: in narrow ReLU networks, the sequence of correlations $(C_{pq}^l)_l$ fails to converge to 1 (Fig. 1), and the pre-activations are far from being Gaussian (Fig. 2).

Finally, the case of $\phi_{2.05}$ put aside, the results regarding the activation functions ϕ_{θ} are consistent between the two runs. This is not the case with tanh and ReLU.

6 Discussion

Generality of Constraints 1 to 4. To ensure that pre-activations follow a Gaussian $\mathcal{N}(0, 1)$ distribution and that the weights in each layer are i.i.d. at initialization, the four constraints outlined in Section 3 must be satisfied. Relaxing these constraints requires either breaking symmetries or addressing more complex problems. Let us consider two examples.

Example 1: instead of making all the pre-activations Gaussian, one may want to impose some other distribution. In this case, the problem to solve would be more difficult: we would have to decompose a non-Gaussian random variable Z into a weighted sum $\frac{1}{\sqrt{n}} \sum_{j=1}^n W_j \phi(X_j)$. In this case, we cannot use Proposition 3, and we would have to make $W_j \phi(X_j)$ belong to a family of random variables stable by multiplication by a constant and by sum, for arbitrary n . If we aim for a non-Gaussian Z , this task is much harder. For a study of infinitely wide neural networks going beyond Gaussian pre-activations, see Peluchetti et al. (2020).

Example 2: instead of assuming that all the weights of a given layer are i.i.d., one may want to initialize them with different distributions or to introduce a dependence structure between them. If the goal remains to obtain Gaussian pre-activations, this kind of generalization should be feasible without drastically changing the constraints we are proposing.

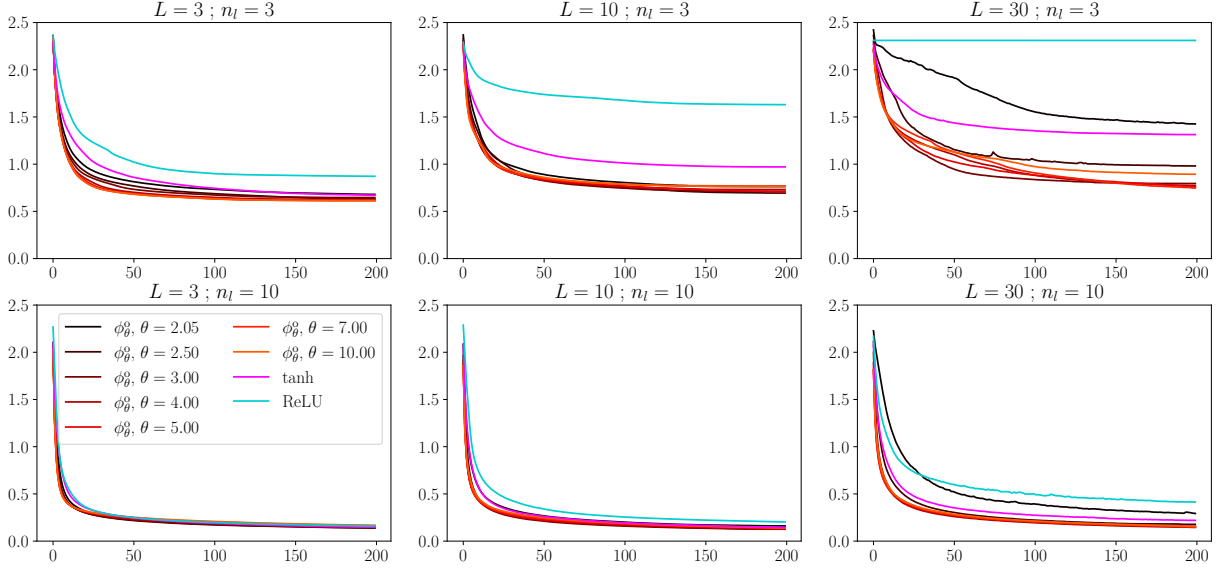


Figure 10: Training loss for a multilayer perceptron, narrow ($n_l \in \{3, 10\}$) and of various depths ($L \in \{3, 10, 30\}$). Training curves averaged over 5 experiments.

Hypothesis of independent pre-activations. In the constraints, we have assumed that the inputs of any layer are independent. This assumption is discussed in Remark 7 and in Appendix B. According to the experimental results presented in Appendix B, we can build specific cases where the dependence between inputs breaks the Gaussianity of the outputted pre-activations, including with our pairs $(\phi_\theta^{o/p}, P_\theta)$.

However, the results are different with ϕ_θ^o and ϕ_θ^p . The difference between Figures 7a and 7b is striking: with ϕ_θ^o , the dependence between pre-activations tends to damage the Gaussianity after a certain number of layers, but with ϕ_θ^p , the Gaussianity of the pre-activations is remarkably well-preserved during propagation. The same kind of result is presented in Appendix B, Figure 11.

Other families of initialization distributions and activation functions. Given the constraints we have derived, we have made a choice to obtain our family of initialization distributions and activation functions: we have decided that the weights should be sampled from a symmetric Weibull distribution $\mathcal{W}(\theta, 1)$. We have made this choice because Weibull distributions meet immediately Constraint 2, and we can modulate their Generalized Weibull Tail parameter easily (see Remark 9).

One may propose another family of initialization distributions, as long as it meets the constraints. However, such a family should be selected wisely: if one chooses a distribution with compact support, or $\text{GWT}(\theta)$ with $\theta \gg 2$, then the related activation function ϕ is likely to be almost linear. Intuitively, if we want $W\phi(X)$ to be $\mathcal{N}(0, 1)$ with $X \sim \mathcal{N}(0, 1)$ and very light-tailed W , then ϕ must “reproduce” the tail of its input X , so ϕ must be approximately linear around infinity.

Preserving a characteristic during propagation or imposing stable fixed points? Previous works have used both ideas: Glorot & Bengio (2010) aim at preserving the variance of the pre-activations, while Poole et al. (2016), Schoenholz et al. (2017) aim at imposing a specific stable fixed point for the correlation map \mathcal{C} . According to the results we have obtained in Section 5.1, it is possible to *approximately* preserve the distribution of the pre-activations when passing through *one* layer. However, according to the results of Section 5.2, a drift can appear after several layers. Therefore, when testing an initialization setup in the real world, with numerical errors and approximations, it is necessary to check the stable fixed points of the monitored characteristic. However, this is not easy to do in practice: without the Gaussian hypothesis, it can be difficult to find the possible limits of $(c_{ab}^l)_l$.

Gaussian pre-activations and Neural Tangent Kernels. With our pair of activation functions and initialization procedure, we have been able to obtain non-asymptotic Edge of Chaos, removing the infinite-width assumption. Since this infinite-width assumption is also fundamental in works on the Neural Tangent Kernels (NTKs) (Jacot et al., 2018), would it be possible to obtain the same kind of results within the NTK setup? We do not think so. On the one hand, the infinite-width limit is used to end up with an NTK that is *constant* during training, in order to provide exact equations of evolution of the trained neural network. On the other hand, in our setup, we only ensure Gaussian pre-activations, and this does not imply that the NTK would be constant during training. Nevertheless, with Gaussian pre-activations, we could expect an improvement in the convergence rate of the neural network towards a stacked Gaussian process, as the widths of the layers tend to infinity. Thus, the NTK regime would be easier to achieve.

A broadly useful technique. Our proposed setup can be readily adopted by practitioners interested in testing the Gaussian hypothesis on problems beyond those considered in this work. The code used here is available on GitHub: <https://github.com/p-wol/gaussian-preact>. One could use this code to train, evaluate, and compare neural networks built using our family of activation functions and initialization distributions against standard choices (such as tanh or ReLU with Gaussian EOC initialization), to assess the impact of enforcing Gaussian pre-activations.

Taking into account the generalization performance. In the EOC framework and ours, a common principle could be discussed and improved. Generalization performance is not taken into account at any step of the reasoning. As we have seen in the training experiments, the main difficulty in our setup is overfitting: as the training loss decreases without obstacles, the test loss ends up being worse than with ReLU and tanh activation functions. To improve these generalization results, one can introduce a separation between the training set and a validation set into the framework.

Precise characterization of the pre-activations distributions \mathcal{D}^l . Finally, finding an accurate and useful characterization of the of the pre-activations distributions \mathcal{D}^l remains an unsolved problem. In the EOC line of work, the problem has been simplified by using the Gaussian hypothesis. However, as shown in the present work, such a simplification is too coarse and leads to inconsistent results. Nevertheless, our approach has its own drawbacks. Namely, we can ensure Gaussian pre-activations only when using specific initialization distributions and activation functions. Thus, we still lack a characterization of the distributions \mathcal{D}^l that is applicable to widely-used networks without rough approximations, and that can be easily used to achieve practical goals, such as finding an optimal initialization scheme. From this perspective, we expect that the problem statement of Section 3.4 will lead to fruitful future research.

Is it desirable to have Gaussian pre-activations? We have presented several results that should help to answer this tough question, but it remains difficult to answer it definitively:

- there is a paradox regarding the ReLU activation. On the one hand, when ReLU is used in narrow and deep perceptrons, the pre-activations are far from being Gaussian, the sequence of correlations does not converge to 1, and training is difficult and unstable. On the other hand, in LeNet-type networks with ReLU, training is easy, and the resulting networks generalize well;
- our activation functions $(\phi_\theta^o)_\theta$ perform quite differently depending on the setup: with $\phi_{2.05}$, LeNet can achieve good training losses, but the training of narrow and deep perceptrons may fail. With $\phi_{10.00}$, we observe opposite results;
- when training narrow networks, the training curves are very different with ϕ_θ^o and ϕ_θ^p . They are difficult to train when using the functions ϕ_θ^p , as well as ReLU (whose pre-activations are far from being Gaussian). But training is feasible and leads often to relatively good results when using ϕ_θ^o .

Therefore, a temporary answer we can give is: with Gaussian pre-activations at initialization and odd activations functions, a neural network is likely to be trainable.

Is the “Gaussian pre-activations hypothesis” a myth or a reality? Our findings reveal that, when using the ReLU activation function in several practical scenarios, it is largely a myth. In contrast, with the tanh activation function, the hypothesis holds true depending on the network’s width: it becomes a reality with a sufficiently large yet reasonable number of neurons per layer. To extend this reality to networks with any layer width, we established a set of constraints that neural network designs must satisfy and proposed solutions to meet these constraints. Consequently, we developed a family of activation functions $(\phi_\theta^p)_\theta$ and initialization distributions P_θ that fulfill these requirements, providing robust foundations for the Gaussian hypothesis and validating it across all tested cases.

Acknowledgements

The project leading to this work has received funding from the European Research Council (ERC) under the European Union’s Horizon 2020 research and innovation program (grant agreement No 834175) and from the French National Research Agency (ANR-21-JSTM-0001) in the framework of the “Investissements d’avenir” program (ANR-15-IDEX-02). This work was granted access to the HPC resources of IDRIS under the allocation 2024-AD011013762R2 made by GENCI. We thank Thomas Duplic for proposing the trick involving the Laplace transform used in Appendix A.1. We would like to thank an anonymous reviewer for pointing out an error in a previous version of the paper, and proposing an example that inspired Example 1 (see App. B).

References

- Zeyuan Allen-Zhu, Yuanzhi Li, and Zhao Song. A convergence theory for deep learning via overparameterization. In *International Conference on Machine Learning*, pp. 242–252. PMLR, 2019.
- Julyan Arbel, Konstantinos Pitas, Mariia Vladimirova, and Vincent Fortuin. A primer on Bayesian neural networks: review and debates. *Statistical Science*, 2024.
- Sanjeev Arora, Nadav Cohen, Wei Hu, and Yuping Luo. Implicit regularization in deep matrix factorization. *Advances in Neural Information Processing Systems*, 32, 2019a.
- Sanjeev Arora, Simon Du, Wei Hu, Zhiyuan Li, and Ruosong Wang. Fine-grained analysis of optimization and generalization for overparameterized two-layer neural networks. In *International Conference on Machine Learning*, pp. 322–332. PMLR, 2019b.
- Sanjeev Arora, Simon S Du, Wei Hu, Zhiyuan Li, Russ R Salakhutdinov, and Ruosong Wang. On exact computation with an infinitely wide neural net. *Advances in Neural Information Processing Systems*, 32, 2019c.
- Krishnakumar Balasubramanian, Larry Goldstein, Nathan Ross, and Adil Salim. Gaussian random field approximation via stein’s method with applications to wide random neural networks. *Applied and Computational Harmonic Analysis*, pp. 101668, 2024.
- Andrea Basteri and Dario Trevisan. Quantitative Gaussian approximation of randomly initialized deep neural networks. *Machine Learning*, 113(9):6373–6393, 2024.
- Patrick Billingsley. *Probability and Measure*. John Wiley & Sons, third edition, 1995.
- Bruno De Finetti. La prévision: ses lois logiques, ses sources subjectives. In *Annales de l’Institut Henri Poincaré*, volume 7, pp. 1–68, 1937.
- Simon Du, Jason Lee, Haochuan Li, Liwei Wang, and Xiyu Zhai. Gradient descent finds global minima of deep neural networks. In *International Conference on Machine Learning*, pp. 1675–1685. PMLR, 2019.
- Benjamin Epstein. Some applications of the Mellin transform in statistics. *The Annals of Mathematical Statistics*, pp. 370–379, 1948.

- Arthur Erdélyi, (Hans Heinrich) Wilhelm Magnus, Fritz Oberhettinger, Francesco Giacomo Tricomi, David Bertin, Watson B. Fulks, A. R. Harvey, Donald L. Thomsen, Jr., Maria A. Weber, E. L. Whitney, and Rosemarie Stampfel. *Higher transcendental functions*, volume I. Bateman Manuscript Project, 1953.
- Stefano Favaro, Boris Hanin, Domenico Marinucci, Ivan Nourdin, and Giovanni Peccati. Quantitative CLTs in deep neural networks. *Probability Theory and Related Fields*, pp. 1–45, 2025.
- Vincent Fortuin. Priors in Bayesian deep learning: A review. *International Statistical Review*, 2022.
- Vincent Fortuin, Adrià Garriga-Alonso, Sebastian W. Ober, Florian Wenzel, Gunnar Ratsch, Richard E Turner, Mark van der Wilk, and Laurence Aitchison. Bayesian neural network priors revisited. In *International Conference on Learning Representations*, 2022.
- Bruno Gabutti and Laura Sacripante. Numerical inversion of the Mellin transform by accelerated series of Laguerre polynomials. *Journal of Computational and Applied Mathematics*, 34(2):191–200, 1991.
- Xavier Glorot and Yoshua Bengio. Understanding the difficulty of training deep feedforward neural networks. In *Proceedings of the 13th International Conference on Artificial Intelligence and Statistics*, pp. 249–256. JMLR Workshop and Conference Proceedings, 2010.
- Izrail Solomonovich Gradshteyn and Iosif Moiseevich Ryzhik. *Table of Integrals, Series, and Products*. Academic Press, eighth edition, 2014.
- Alex Graves. Practical variational inference for neural networks. *Advances in Neural Information Processing Systems*, 24, 2011.
- Boris Hanin and Mihai Nica. Finite depth and width corrections to the neural tangent kernel. In *International Conference on Learning Representations*, 2020.
- Soufiane Hayou, Arnaud Doucet, and Judith Rousseau. On the impact of the activation function on deep neural networks training. In *International Conference on Machine Learning*, pp. 2672–2680. PMLR, 2019.
- Kaiming He, Xiangyu Zhang, Shaoqing Ren, and Jian Sun. Delving deep into rectifiers: Surpassing human-level performance on imagenet classification. In *Proceedings of the IEEE international conference on computer vision*, pp. 1026–1034, 2015.
- Matthew D Hoffman, David M Blei, Chong Wang, and John Paisley. Stochastic variational inference. *Journal of Machine Learning Research*, 2013.
- Arthur Jacot, Franck Gabriel, and Clément Hongler. Neural tangent kernel: Convergence and generalization in neural networks. *Advances in Neural Information Processing Systems*, 31, 2018.
- Diederik P Kingma and Jimmy L Ba. Adam: A method for stochastic optimization. In *International Conference on Learning Representations*, 2015.
- Günter Klambauer, Thomas Unterthiner, Andreas Mayr, and Sepp Hochreiter. Self-normalizing neural networks. *Advances in Neural Information Processing Systems*, 30, 2017.
- Andrey Kolmogoroff. Confidence limits for an unknown distribution function. *The Annals of Mathematical Statistics*, 12(4):461–463, 1941.
- Yann LeCun, Léon Bottou, Yoshua Bengio, and Patrick Haffner. Gradient-based learning applied to document recognition. *Proceedings of the IEEE*, 86(11):2278–2324, 1998.
- Jaehoon Lee, Yasaman Bahri, Roman Novak, Samuel S Schoenholz, Jeffrey Pennington, and Jascha Sohl-Dickstein. Deep Neural Networks as Gaussian Processes. In *International Conference on Learning Representations*, 2018.
- Jaehoon Lee, Lechao Xiao, Samuel Schoenholz, Yasaman Bahri, Roman Novak, Jascha Sohl-Dickstein, and Jeffrey Pennington. Wide neural networks of any depth evolve as linear models under gradient descent. *Advances in Neural Information Processing Systems*, 32, 2019.

- Mufan Li, Mihai Nica, and Dan Roy. The neural covariance sde: Shaped infinite depth-and-width networks at initialization. *Advances in Neural Information Processing Systems*, 35:10795–10808, 2022.
- Haitao Mao, Xu Chen, Qiang Fu, Lun Du, Shi Han, and Dongmei Zhang. Neuron campaign for initialization guided by information bottleneck theory. In *Proceedings of the 30th ACM International Conference on Information & Knowledge Management*, pp. 3328–3332, 2021.
- James Martens, Andy Ballard, Guillaume Desjardins, Grzegorz Swirszcz, Valentin Dalibard, Jascha Sohl-Dickstein, and Samuel S Schoenholz. Rapid training of deep neural networks without skip connections or normalization layers using deep kernel shaping. *arXiv preprint arXiv:2110.01765*, 2021.
- Alexander G de G Matthews, Jiri Hron, Mark Rowland, Richard E Turner, and Zoubin Ghahramani. Gaussian process behaviour in wide deep neural networks. In *International Conference on Learning Representations*, 2018.
- Radford M Neal. *Bayesian learning for neural networks*, volume 118 of *Lecture Notes in Statistics*. Springer, New York, 1996.
- Lorenzo Noci, Gregor Bachmann, Kevin Roth, Sebastian Nowozin, and Thomas Hofmann. Precise characterization of the prior predictive distribution of deep ReLU networks. *Advances in Neural Information Processing Systems*, 34:20851–20862, 2021.
- Yann Ollivier. Online natural gradient as a Kalman filter. *Electronic Journal of Statistics*, 12(2):2930–2961, 2018.
- Theodore Papamarkou, Maria Skoularidou, Konstantina Palla, Laurence Aitchison, Julyan Arbel, David Dunson, Maurizio Filippone, Vincent Fortuin, Philipp Hennig, Aliaksandr Hubin, Alexander Immer, Theofanis Karaletsos, Mohammad Emtiyaz Khan, Agustinus Kristiadi, Yingzhen Li, Jose Miguel Hernandez Lobato, Stephan Mandt, Christopher Nemeth, Michael A. Osborne, Tim G. J. Rudner, David Rügamer, Yee Whye Teh, Max Welling, Andrew Gordon Wilson, and Ruqi Zhang. Position Paper: Bayesian Deep Learning is Needed in the Age of Large-Scale AI. In *International Conference on Machine Learning*, pp. 39556–39586. PMLR, 2024.
- Razvan Pascanu, Tomas Mikolov, and Yoshua Bengio. On the difficulty of training recurrent neural networks. In *International Conference on Machine Learning*, pp. 1310–1318. PMLR, 2013.
- Stefano Peluchetti, Stefano Favaro, and Sandra Fortini. Stable behaviour of infinitely wide deep neural networks. In *International Conference on Artificial Intelligence and Statistics*, pp. 1137–1146. PMLR, 2020.
- Ben Poole, Subhaneil Lahiri, Maithra Raghu, Jascha Sohl-Dickstein, and Surya Ganguli. Exponential expressivity in deep neural networks through transient chaos. *Advances in Neural Information Processing Systems*, 29, 2016.
- Hadi Pouransari, Zhucheng Tu, and Oncel Tuzel. Least squares binary quantization of neural networks. In *Proceedings of the IEEE/CVF Conference on Computer Vision and Pattern Recognition Workshops*, pp. 698–699, 2020.
- Daniel A. Roberts, Sho Yaida, and Boris Hanin. *The Principles of Deep Learning Theory: An Effective Theory Approach to Understanding Neural Networks*. Cambridge University Press, 2022.
- Andrew M Saxe, Yamini Bansal, Joel Dapello, Madhu Advani, Artemy Kolchinsky, Brendan D Tracey, and David D Cox. On the information bottleneck theory of deep learning. *Journal of Statistical Mechanics: Theory and Experiment*, 2019(12):124020, 2019.
- Samuel S Schoenholz, Justin Gilmer, Surya Ganguli, and Jascha Sohl-Dickstein. Deep information propagation. In *International Conference on Learning Representations*, 2017.
- Mariia Selezнова and Gitta Kutyniok. Analyzing finite neural networks: Can we trust neural tangent kernel theory? In *Mathematical and Scientific Machine Learning*, pp. 868–895. PMLR, 2022.

- Ravid Shwartz-Ziv and Naftali Tishby. Opening the black box of deep neural networks via information. *arXiv preprint arXiv:1703.00810*, 2017.
- Vincent Sitzmann, Julien Martel, Alexander Bergman, David Lindell, and Gordon Wetzstein. Implicit neural representations with periodic activation functions. *Advances in Neural Information Processing Systems*, 33:7462–7473, 2020.
- Nikolay Smirnov. Table for estimating the goodness of fit of empirical distributions. *The Annals of Mathematical Statistics*, 19(2):279–281, 1948.
- P S Theocaris and A C Chrysakis. Numerical inversion of the Mellin transform. *IMA Journal of Applied Mathematics*, 20(1):73–83, 1977.
- Naftali Tishby. The information bottleneck method. In *Proc. 37th Annual Allerton Conference on Communications, Control and Computing, 1999*, pp. 368–377, 1999.
- Edward Charles Titchmarsh. *Introduction to the theory of Fourier integrals*. The Clarendon Press, Oxford, 2nd edition, 1937.
- Dario Trevisan. Wide deep neural networks with Gaussian weights are very close to Gaussian processes. *arXiv preprint arXiv:2312.11737*, 2023.
- Mariia Vladimirova, Jakob Verbeek, Pablo Mesejo, and Julyan Arbel. Understanding priors in Bayesian neural networks at the unit level. In *International Conference on Machine Learning*, pp. 6458–6467. PMLR, 2019.
- Mariia Vladimirova, Julyan Arbel, and Stéphane Girard. Bayesian neural network unit priors and generalized Weibull-tail property. In *Asian Conference on Machine Learning*, pp. 1397–1412. PMLR, 2021.
- Florian Wenzel, Kevin Roth, Bastiaan Veeling, Jakub Swiatkowski, Linh Tran, Stephan Mandt, Jasper Snoek, Tim Salimans, Rodolphe Jenatton, and Sebastian Nowozin. How good is the Bayes posterior in deep neural networks really? In *International Conference on Machine Learning*, pp. 10248–10259. PMLR, 2020.
- Sho Yaida. Non-gaussian processes and neural networks at finite widths. In *Mathematical and Scientific Machine Learning*, pp. 165–192. PMLR, 2020.
- Guodong Zhang, Aleksandar Botev, and James Martens. Deep learning without shortcuts: Shaping the kernel with tailored rectifiers. In *International Conference on Learning Representations*, 2022.

A Activation function with infinite number of stable fixed points for \mathcal{V}

A.1 Proof that \mathcal{V} admits an infinite number of fixed points when using $\phi = \varphi_{\delta,\omega}$

Proposition 2. For any $\delta \in (0, 1]$ and $\omega > 0$, let us pose the activation function $\phi = \varphi_{\delta,\omega}$. We consider the sequence $(v^l)_l$ defined by:

$$\begin{aligned} \forall l \geq 0, \quad v^{l+1} &= \sigma_w^2 \int \varphi_{\delta,\omega} \left(\sqrt{v^l} z \right)^2 \mathcal{D}z + \sigma_b^2, \\ v^0 &\in \mathbb{R}_*^+. \end{aligned} \quad (52)$$

Then there exists $\sigma_w > 0$, $\sigma_b \geq 0$, and a strictly increasing sequence of stable fixed points $(v_k^*)_{k \in \mathbb{Z}}$ of the recurrence Equation (52).

Proof. Let us define:

$$\begin{aligned} \tilde{\mathcal{V}}(v) &:= \frac{1}{v} \mathcal{V}(v | \sigma_w = 1, \sigma_b = 0), \\ \text{so we have:} \quad \mathcal{V}(v | \sigma_w, \sigma_b) &= \sigma_w^2 v \tilde{\mathcal{V}}(v) + \sigma_b^2. \end{aligned} \quad (53)$$

In the following, we use a simplified notation: $\mathcal{V}(v) = \mathcal{V}(v | \sigma_w, \sigma_b)$.

Our goal is to find a sequence $(v_k^*)_{k \in \mathbb{Z}}$, σ_w and σ_b such that:

$$\forall k \in \mathbb{Z}, \quad \mathcal{V}(v_k^*) = v_k^* \quad \text{and} \quad \mathcal{V}'(v_k^*) \in (-1, 1),$$

which would ensure that all v_k^* are stable fixed points of \mathcal{V} . In order to understand how to build the sequence $(v_k^*)_{k \in \mathbb{Z}}$, let us consider $v > 0$. Let $\sigma_b^2 = 0$ and $\sigma_w^2 = 1/\tilde{\mathcal{V}}(v)$. So we have:

$$\mathcal{V}(v) = v.$$

So, any $v > 0$ can possibly be a fixed point if we tune σ_w accordingly. We just have to find a $v > 0$ such that: $\mathcal{V}'(v) \in (-1, 1)$, with:

$$\mathcal{V}'(v) = \frac{1}{\tilde{\mathcal{V}}(v)} (\tilde{\mathcal{V}}(v) + v \tilde{\mathcal{V}}'(v)) = 1 + \tilde{\mathcal{V}}'_e(\ln(v)), \quad (54)$$

where $\tilde{\mathcal{V}}_e : r \mapsto \ln(\tilde{\mathcal{V}}(\exp(r)))$. So, knowing that $\tilde{\mathcal{V}}_e$ is \mathcal{C}^1 and periodic, it is sufficient to prove that it is not constant to ensure that we can extract one v_0^* such that $\mathcal{V}'(v_0^*) \in (-1, 1)$. Then, by periodicity of $\tilde{\mathcal{V}}_e$, we can build a sequence of stable fixed points $(v_k^*)_{k \in \mathbb{Z}}$.

We have:

$$\begin{aligned} \tilde{\mathcal{V}}(v) &= \frac{1}{v} \int_{-\infty}^{\infty} \varphi_{\delta,\omega}(\sqrt{v}z)^2 \mathcal{D}z = \int_{-\infty}^{\infty} z^2 \exp\left(2\frac{\delta}{\omega} \sin(\omega \ln |\sqrt{v}z|)\right) \mathcal{D}z \\ &= 2 \int_0^{\infty} z^2 \exp\left(2\frac{\delta}{\omega} \sin(\omega \ln(\sqrt{v}z))\right) \mathcal{D}z = 2 \int_0^{\infty} z^2 \exp\left(2\frac{\delta}{\omega} \sin\left(\frac{\omega}{2} \ln v + \omega \ln z\right)\right) \mathcal{D}z. \end{aligned}$$

Lemma 1. $\tilde{\mathcal{V}}$ is not constant.

Proof.

$$\begin{aligned} \tilde{\mathcal{V}}(v) &= \frac{1}{\sqrt{2\pi}} \frac{2}{v^{3/2}} \int_0^{\infty} z^2 \exp\left(2\frac{\delta}{\omega} \sin(\omega \ln z)\right) \exp\left(-\frac{z^2}{2v}\right) dz \\ &= \frac{1}{\sqrt{2\pi}} \frac{2}{v^{3/2}} \int_0^{\infty} \frac{z}{2\sqrt{z}} \exp\left(2\frac{\delta}{\omega} \sin(\omega \ln \sqrt{z})\right) \exp\left(-\frac{z}{2v}\right) dz \\ &= \frac{1}{\sqrt{2\pi}} v^{-3/2} \mathcal{L}[\varphi_{\delta,\omega}(\sqrt{z})] \left(\frac{1}{2v}\right), \end{aligned}$$

where \mathcal{L} is the Laplace transform.

Let us suppose that $\tilde{\mathcal{V}}$ is constant: $\forall v > 0, \tilde{\mathcal{V}}(v) = c$. So, if we pose $v \leftarrow \frac{1}{2v}$, we have:

$$\forall v > 0, \quad c = \frac{2}{\sqrt{\pi}} v^{3/2} \mathcal{L} [\varphi_{\delta, \omega}(\sqrt{z})] (v),$$

that is:

$$\mathcal{L} [\varphi_{\delta, \omega}(\sqrt{z})] (v) = \frac{c\sqrt{\pi}}{2} v^{-3/2}.$$

Since the function $z \mapsto \varphi_{\delta, \omega}(\sqrt{z})$ is continuous on \mathbb{R}^+ , then, almost everywhere (see Thm. 22.2, Billingsley, 1995):

$$\varphi_{\delta, \omega}(\sqrt{z}) = \frac{c\sqrt{\pi}}{2} \mathcal{L}^{-1}[v^{-3/2}](z) = c\sqrt{z},$$

which is impossible for $\delta \in (0, 1]$. Hence the result. \square

The function $\tilde{\mathcal{V}}_e : r \mapsto \ln(\tilde{\mathcal{V}}(\exp(r)))$ is continuous and $\frac{4\pi}{\omega}$ -periodic:

$$\tilde{\mathcal{V}}_e(r) = \ln \left[2 \int_0^\infty z^2 \exp \left(2 \frac{\delta}{\omega} \sin \left(\frac{\omega}{2} r + \omega \ln z \right) \right) \mathcal{D}z \right],$$

so $\tilde{\mathcal{V}}_e$ is lower and upper bounded and reach its bounds (and, by Lemma 1, these bounds are different). We define:

$$\begin{aligned} \tilde{\mathcal{V}}_e^+ &= \max \tilde{\mathcal{V}}_e & r_0^+ &= \inf \{ r > 0 : \tilde{\mathcal{V}}_e(r) = \tilde{\mathcal{V}}_e^+ \}, \\ \tilde{\mathcal{V}}_e^- &= \min \tilde{\mathcal{V}}_e & r_0^- &= \inf \{ r > r_0^+ : \tilde{\mathcal{V}}_e(r) = \tilde{\mathcal{V}}_e^- \}. \end{aligned}$$

By continuity, $\tilde{\mathcal{V}}_e(r_0^+) = \tilde{\mathcal{V}}_e^+$ and $\tilde{\mathcal{V}}_e(r_0^-) = \tilde{\mathcal{V}}_e^-$. Since $\tilde{\mathcal{V}}^+ > \tilde{\mathcal{V}}^-$ and $\tilde{\mathcal{V}}_e$ is \mathcal{C}^1 , then there exists $r_0^* \in (r_0^+, r_0^-)$ such that $\tilde{\mathcal{V}}_e'(r_0^*) \in (-2, 0)$.

Since $\tilde{\mathcal{V}}_e$ is $\frac{4\pi}{\omega}$ -periodic, we can define a sequence $(r_k^*)_{k \in \mathbb{Z}}$ such that:

$$\begin{aligned} r_k^* &:= r_0^* + \frac{4k\pi}{\omega} \\ \tilde{\mathcal{V}}_e(r_k^*) &= \tilde{\mathcal{V}}_e(r_0^*) =: \tilde{\mathcal{V}}_e^0 \\ \tilde{\mathcal{V}}_e'(r_k^*) &= \tilde{\mathcal{V}}_e'(r_0^*) \in (-2, 0). \end{aligned}$$

So, by using Eqn. (53) and Eqn. (54) with $\sigma_b^2 = 0$ and $\sigma_w^2 = 1/\exp(\tilde{\mathcal{V}}_e^0)$:

$$\begin{aligned} v_k^* &:= \exp(r_k^*), \\ \mathcal{V}(v_k^*) &= \frac{1}{\exp(\tilde{\mathcal{V}}_e^0)} v_k^* \tilde{\mathcal{V}}(v_k^*) = v_k^* \\ \mathcal{V}'(v_k^*) &= 1 + \tilde{\mathcal{V}}_e'(r_0^*) \in (-1, 1). \end{aligned}$$

Thus, $(v_k^*)_{k \in \mathbb{Z}}$ is a sequence of stable fixed points of $\mathcal{V}(\cdot | \sigma_w, \sigma_b)$ for well-chosen σ_w and σ_b . \square

A.2 Practical computation of σ_w^2

We propose a practical method to ensure that $\mathcal{V}(\cdot | \sigma_w, \sigma_b = 0)$ admits an infinite number of stable fixed points when using activation function $\phi = \varphi_{\delta, \omega}$.

In order to achieve this goal, we build $\sigma_w^2 = \sigma_\omega^2$ in the following way:

$$\begin{aligned}\mathcal{V}_{\text{low}} &:= 2 \int_0^\infty z^2 \exp\left(-2\frac{\delta}{\omega} \sin(\omega \ln(z))\right) \mathcal{D}z \\ \mathcal{V}_{\text{upp}} &:= 2 \int_0^\infty z^2 \exp\left(2\frac{\delta}{\omega} \sin(\omega \ln(z))\right) \mathcal{D}z, \\ \sigma_\omega^2 &:= \left[\frac{\mathcal{V}_{\text{low}} + \mathcal{V}_{\text{upp}}}{2}\right]^{-1}.\end{aligned}$$

In practice, for $\delta = 0.99$, we obtain σ_ω for $\omega \in \{2, 3, 6\}$:

$$\sigma_2 \approx 0.879, \quad \sigma_3 \approx 0.945, \quad \sigma_6 \approx 0.987.$$

B Discussion about the independence of the pre-activations

In Proposition 3 and Constraint 1, we assume that, for any layer l , its inputs $(Z_j^l)_j$ are independent. This does not hold in full generality:

Example 1. Let $X \sim \mathcal{N}(0, 1)$ be some random input of a two-layer neural network. We perform the following operation:

$$Z = \frac{1}{\sqrt{2}} [W_1^2 \phi(W_1^1 X) + W_2^2 \phi(W_2^1 X)],$$

where $(W_1^1, W_2^1, W_1^2, W_2^2)$ be i.i.d. random variables samples from some distribution \mathcal{P} , and ϕ is some activation function.

Let $\mathcal{P} = \mathcal{R}$, the Rademacher distribution, i.e., if $W \sim \mathcal{R}$, then $W = \pm 1$ with probability $1/2$. Let $\phi = \text{Id}$. Then we have: $Y_1 := W_1^1 X \sim \mathcal{N}(0, 1)$ and $Y_2 := W_2^1 X \sim \mathcal{N}(0, 1)$. But they are not independent:

$$W_1^2 W_1^1 X + W_2^2 W_2^1 X = (W_1' + W_2')X,$$

where $W_1^2 W_1^1$ and $W_2^2 W_2^1$ are two independent Rademacher random variables. So, $Z = 0$ with probability $1/2$. So, Z is not Gaussian.

In this example, we build a non-Gaussian random variable with a minimal neural network, in which we construct two dependent random variables. So, we should pay attention to this phenomenon when propagating the pre-activations in a neural network.

One should note that the structure of dependence of $W_1^2 W_1^1 X$ and $W_2^2 W_2^1 X$ does not involve their correlation (which is zero), and yet breaks the Gaussianity of their sum. So, in order to obtain a theoretical result about the distribution of Z , we should study finer aspects of the dependence structure.

But, on the practical side, we want to answer the question: to which extent does the relation of dependence between the pre-activations $(Z_j^l)_j$ affect the Gaussianity of $(Z_i^{l+1})_i$?

In order to answer this question, we propose a series of experiments on a two-layer neural network. We consider a vector of inputs $\mathbf{X} \in \mathbb{R}^{n_0}$, where the $(X_j)_{1 \leq j \leq n_0}$ are $\mathcal{N}(0, 1)$ and i.i.d. The scalar outputted by the network is:

$$Z = \frac{1}{\sqrt{n_1}} \mathbf{W}^2 \phi\left(\frac{1}{\sqrt{n_0}} \mathbf{W}^1 \mathbf{X}\right),$$

where the weights $\mathbf{W}^1 \in \mathbb{R}^{n_1 \times n_0}$ and $\mathbf{W}^2 \in \mathbb{R}^{1 \times n_1}$ are i.i.d.

We test this setup with different initialization distributions \mathcal{P} and activation functions ϕ :

- usual ones: $\phi = \tanh$ or ReLU , $\mathcal{P} = \mathcal{N}(0, \sigma_w^2)$, where σ_w^2 is such that the pair $(\sigma_w^2, \sigma_b^2 = 0.01)$ lies at the EOC;

- ours: $\phi = \phi_\theta$, $P = P_\theta = \mathcal{W}(\theta, 1)$.

We study three cases:

- unfavorable case: $n_0 = 1$, various $n_1 \in [1, 10]$;
the intermediary features $\mathbf{W}^1 \mathbf{X}$ are weakly “mixed”, so it is credible that they lead to an output that is far from being Gaussian;
- favorable case: $n_1 = 2$, various $n_0 \in [1, 10]$;²¹
the intermediary features $\mathbf{W}^1 \mathbf{X}$ are “mixed” with an increasing rate as n_0 increases;
- same-width case: $n_0 = n_1$.

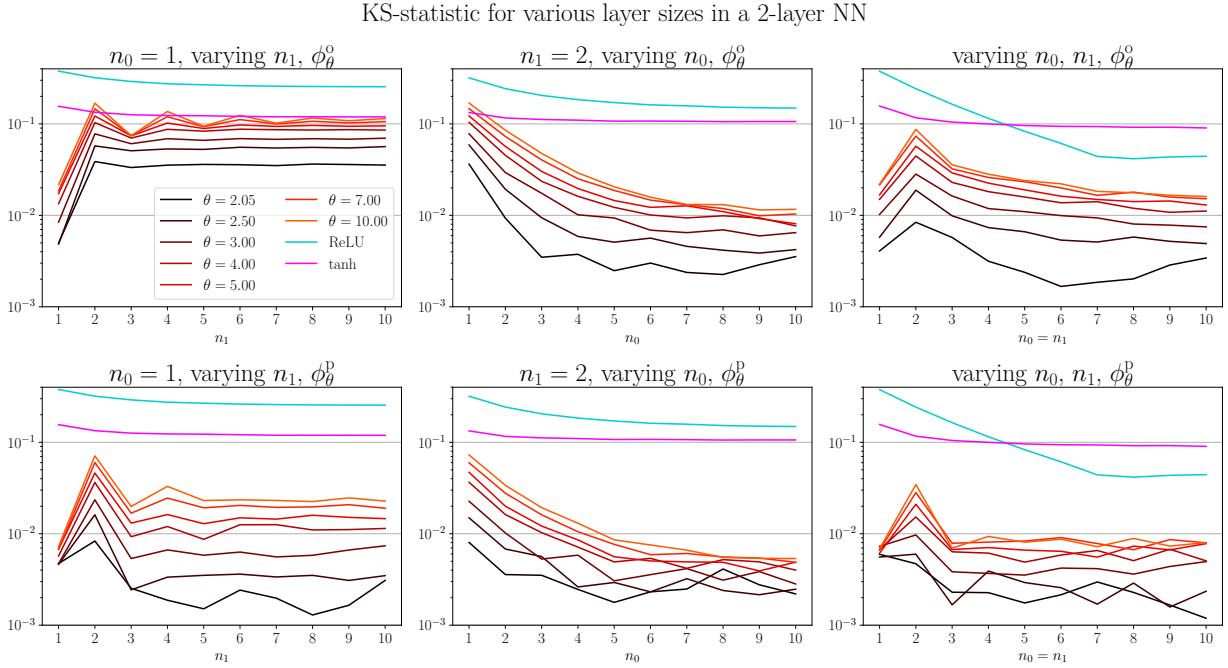


Figure 11: Evolution of the distance of the standardized distribution of Z to the $\mathcal{N}(0, 1)$ according to the Kolmogorov–Smirnov statistic. Weight initialization is $\mathcal{W}(\theta, 1)$ when using $\phi = \phi_\theta$ and is Gaussian according to the EOC when using $\phi = \tanh$ or ReLU . For each point, we have computed the KS-statistic over 200 000 samples of $(\mathbf{X}, \mathbf{W}^1, \mathbf{W}^2)$. In the first row, we have plotted the results for the **odd** activation functions ϕ_θ^o . In the second row, we have plotted the results for the **positive** activation functions ϕ_θ^p .

According to Figure 11:

- unfavorable case (1st graph, $n_0 = 1$): Z is far from being Gaussian for ReLU , \tanh , and the ϕ_θ^o , but is much better for the ϕ_θ^p , especially with a small θ ;
- favorable case (2nd graph, $n_1 = 2$): Z is closer to be Gaussian with our setups $(P_\theta, \phi_\theta^{o/p})$ than with $\phi = \tanh$ or ReLU , especially with larger n_1 ;
- same-width case (3rd graph, $n = n_0 = n_1$): the larger the width n , the closer Z is to being Gaussian. For a fixed n , the distribution of Z is closer to a Gaussian with smaller θ . When we use $(P_\theta, \phi_\theta^{o/p})$, we are close to the performance of \tanh or better.

²¹The case $n_1 = 1$ is trivial: there is no sum of dependent random variables in the second layer.

The case $n_0 = n_1$ is the most realistic one: usually, the sizes of the layers of a neural network are of the same order of magnitude. In this case, our setup is better than or equivalent to the ones with tanh or ReLU.

Mixing of inputs and interference phenomenon. We see in Figure 11 that, in every graph, setups with small θ lead to better results than the ones with large θ . This observation could be explained by Example 1. In this example, the inputs are weakly “mixed”: since X_0 is multiplied by a Rademacher random variable, it is possible to partially reconstruct X_0 after the first layer, and then build destructive interference (leading to an output $Z = 0$ half of the time).

So, if we want to avoid this “interference” phenomenon, we should use initialization distributions and activation functions such that every layer “mixes” strongly the inputs. Notably, initialization distributions should be far from being a combination of Dirac distributions. Typically, $P_{\theta=10}$ is close to the Rademacher distribution (see Fig. 5a).

Finally, this phenomenon can be greatly reduced by using our family $(\phi_\theta^p)_\theta$ of positive activation functions (see second row of Figure 11).

C Constraints on the product of two random variables

Proposition 4 (Density of a product of random variables at 0). *Let W, Y be two independent non-negative random variables and $Z = WY$. Let f_W, f_Y, f_Z be their respective density. Assuming that f_Y is continuous at 0 with $f_Y(0) > 0$, we have:*

$$\text{if } \lim_{w \rightarrow 0} \int_w^\infty \frac{f_W(t)}{t} dt = \infty, \quad \text{then } \lim_{z \rightarrow 0} f_Z(z) = \infty. \quad (55)$$

Moreover, if f_Y is bounded:

$$\text{if } \int_0^\infty \frac{f_W(t)}{t} dt < \infty, \quad \text{then } f_Z(0) = f_Y(0) \int_0^\infty \frac{f_W(t)}{t} dt. \quad (56)$$

Proof. Let $z, z_0 > 0$:

$$\begin{aligned} f_Z(z) &= \int_0^\infty f_Y(t) \frac{1}{t} f_W\left(\frac{z}{t}\right) dt \\ &\geq \int_0^{z_0} f_Y(t) \frac{1}{t} f_W\left(\frac{z}{t}\right) dt \geq \inf_{[0, z_0]} f_Y \cdot \int_0^{z_0} \frac{1}{t} f_W\left(\frac{z}{t}\right) dt \geq \inf_{[0, z_0]} f_Y \cdot \int_{z/z_0}^\infty \frac{f_W(t)}{t} dt. \end{aligned}$$

Let us take $z_0 = \sqrt{z}$. We have:

$$f_Z(z) \geq \inf_{[0, \sqrt{z}]} f_Y \cdot \int_{\sqrt{z}}^\infty \frac{f_W(t)}{t} dt.$$

Then we take the limit $z \rightarrow 0$, hence:

- if $\int_0^\infty \frac{f_W(t)}{t} dt = \infty$, then: $\lim_{z \rightarrow 0} f_Z(z) = \infty$, which achieves (55);
- if $\int_0^\infty \frac{f_W(t)}{t} dt < \infty$, then: $f_Z(0) \geq f_Y(0) \int_0^\infty \frac{f_W(t)}{t} dt$, which achieves one half of (56);

Let us prove the second half of (56). Let $z, z_0 > 0$:

$$\begin{aligned} f_Z(z) &= \int_0^\infty f_Y(t) \frac{1}{t} f_W\left(\frac{z}{t}\right) dt \\ &= \int_0^{z_0} f_Y(t) \frac{1}{t} f_W\left(\frac{z}{t}\right) dt + \int_{z_0}^\infty f_Y(t) \frac{1}{t} f_W\left(\frac{z}{t}\right) dt \\ &\leq \sup_{[0, z_0]} f_Y \cdot \int_{z/z_0}^\infty \frac{f_W(t)}{t} dt + \int_1^\infty f_Y(z_0 t) \frac{1}{t} f_W\left(\frac{z}{z_0 t}\right) dt \end{aligned}$$

Let $z_0 = \sqrt{z}$. We have:

$$f_Z(z) \leq \sup_{[0, \sqrt{z}]} f_Y \cdot \int_{\sqrt{z}}^{\infty} \frac{f_W(t)}{t} dt + \int_1^{\infty} f_Y(\sqrt{z}t) \frac{1}{t} f_W\left(\frac{\sqrt{z}}{t}\right) dt,$$

where:

$$\int_1^{\infty} f_Y(\sqrt{z}t) \frac{1}{t} f_W\left(\frac{\sqrt{z}}{t}\right) dt \leq \|f_Y\|_{\infty} \int_1^{\infty} \frac{1}{t} f_W\left(\frac{\sqrt{z}}{t}\right) dt \leq \|f_Y\|_{\infty} \int_0^{\sqrt{z}} \frac{f_W(t)}{t} dt.$$

According to the hypotheses, we have, as $z \rightarrow 0$:

$$\sup_{[0, \sqrt{z}]} f_Y \rightarrow f_Y(0), \quad \int_{\sqrt{z}}^{\infty} \frac{f_W(t)}{t} dt \rightarrow \int_0^{\infty} \frac{f_W(t)}{t} dt, \quad \int_0^{\sqrt{z}} \frac{f_W(t)}{t} dt \rightarrow 0,$$

hence the result. \square

D Activation functions with vertical tangent at 0

In the following lemma, we show that if we want the activation Y to have a density that is 0 at 0, then the activation function ϕ should have a vertical tangent at 0. G plays the role of pre-activation.

Lemma 2. *Let ϕ be a function transforming a Gaussian random variable $G \sim \mathcal{N}(0, 1)$ into a symmetrical random variable Y with a density f_Y such that $f_Y(0) = 0$. That is, $Y = \phi(G)$. Then ϕ has a vertical tangent at 0.*

Proof. We have:

$$\phi(x) = F_Y^{-1}(F_G(x)),$$

where F_G and F_Y are the respective CDFs of G and Y .

Thus:

$$\phi'(x) = F'_G(x) \frac{1}{F'_Y(F_Y^{-1}(F_G(x)))}$$

Therefore:

$$\phi'(0) = F'_G(0) \frac{1}{F'_Y(F_Y^{-1}(F_G(0)))} = \frac{1}{\sqrt{2\pi}} \frac{1}{F'_Y(F_Y^{-1}(1/2))} = \frac{1}{\sqrt{2\pi}} \frac{1}{F'_Y(0)} = \infty.$$

\square

E The Mellin transform

E.1 Generalities

We assume that $G = WY \sim \mathcal{N}(0, 1)$. Let us consider the random variables $|W|$, $|Y|$ and $|G| = |W| \cdot |Y|$. Let $f_{|W|}$, $f_{|Y|}$ and $f_{|G|}$ be their densities. Under integrability conditions, we can express the density $f_{|G|}$ of the product $|G| = |W||Y|$ with the product-convolution operator \ast :

$$f_{|G|}(z) = (f_{|W|} \ast f_{|Y|})(z), \quad \text{where} \quad (f_{|W|} \ast f_{|Y|})(z) = \int_0^{\infty} f_{|W|}\left(\frac{z}{t}\right) f_{|Y|}(t) \frac{1}{t} dt.$$

We can also express the CDF of $|G|$ this way:

$$F_{|G|}(z) = \int_0^{\infty} F_{|W|}\left(\frac{z}{t}\right) f_{|Y|}(t) dt. \quad (57)$$

Then, we can use the following property of the Mellin transform \mathcal{M} :

$$\mathcal{M}f_{|G|} = (\mathcal{M}f_{|W|}) \cdot (\mathcal{M}f_{|Y|}), \quad \text{where} \quad (\mathcal{M}f)(t) = \int_0^\infty x^{t-1} f(x) dx.$$

In short, \mathcal{M} transforms a product-convolution into a product in the same manner as the Fourier transform \mathcal{F} transforms a convolution into a product. We have then:

$$f_{|Y|}(y) := \mathcal{M}^{-1} \left[\frac{\mathcal{M}f_{|G|}}{\mathcal{M}f_{|W|}} \right] (y).$$

Then, by symmetry, we can obtain f_Y from $f_{|Y|}$. However, while $\mathcal{M}f_{|G|}$ and $\mathcal{M}f_{|W|}$ are easy to compute, the inverse Mellin transform \mathcal{M}^{-1} seems to be analytically untractable in this case:

$$\begin{aligned} (\mathcal{M}f_{|G|})(s) &= \frac{2^{\frac{s}{2}-\frac{1}{2}} \Gamma(\frac{s}{2})}{\sqrt{\pi}}, & (\mathcal{M}f_{|W|})(s) &= \Gamma\left(\frac{s-1}{\theta} + 1\right), \\ \text{so: } \frac{(\mathcal{M}f_{|G|})(s)}{(\mathcal{M}f_{|W|})(s)} &= \frac{1}{\sqrt{\pi}} \frac{2^{\frac{s}{2}-\frac{1}{2}} \Gamma(\frac{s}{2})}{\Gamma\left(\frac{s-1}{\theta} + 1\right)}. \end{aligned}$$

E.2 Numerical inversion of the Mellin transform

Computation of $f_{|Y|}$ by numerical inverse Mellin transform. The Mellin transform of a function can be inverted by using Laguerre polynomials. Specifically, we use the method proposed by [Theocaris & Chrysakis \(1977\)](#) and slightly accelerated by the numerical procedure of [Gabutti & Sacripante \(1991\)](#):

$$(\mathcal{M}^{-1}f)(z) = e^{-\frac{z}{2}} \sum_{k=0}^{\infty} c_{k+1} L_k\left(\frac{z}{2}\right), \quad \text{with } c_k := \sum_{n=1}^k \binom{k-1}{n-1} (-1)^{n-1} \frac{f(n)}{2^n \Gamma(n)}, \quad (58)$$

where the $(L_k)_k$ are the Laguerre polynomials (see Section 7.41, [Gradshteyn & Ryzhik, 2014](#)).

Experiments. A common way of computing the inverse Mellin transform consists of using Equation (58). Specifically, the sequence $(c_k)_k$ must be computed.

In order to compute the density f_Y of Q_θ with $\theta = 2.05$, we have computed numerically $(c_k)_k$ for $k \in [1, 500]$. The results are plotted in Figure 12. We have tested three methods to compute the c_k :

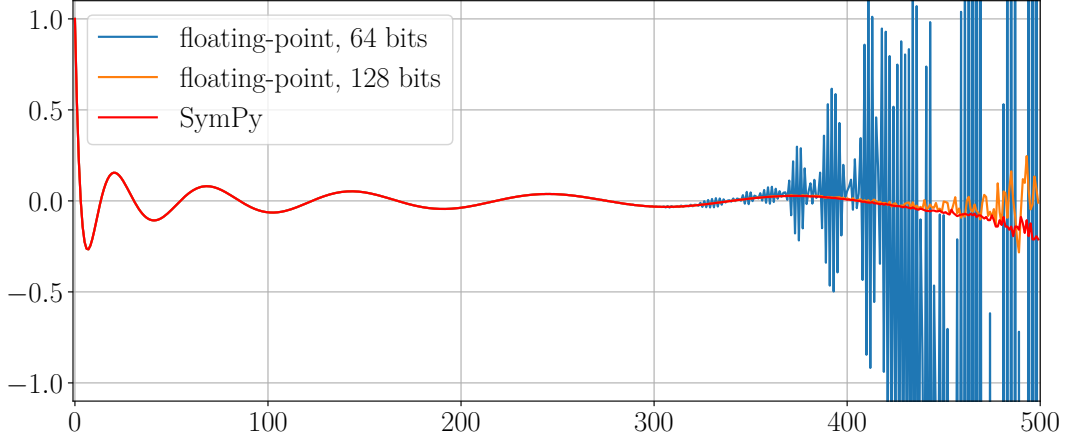
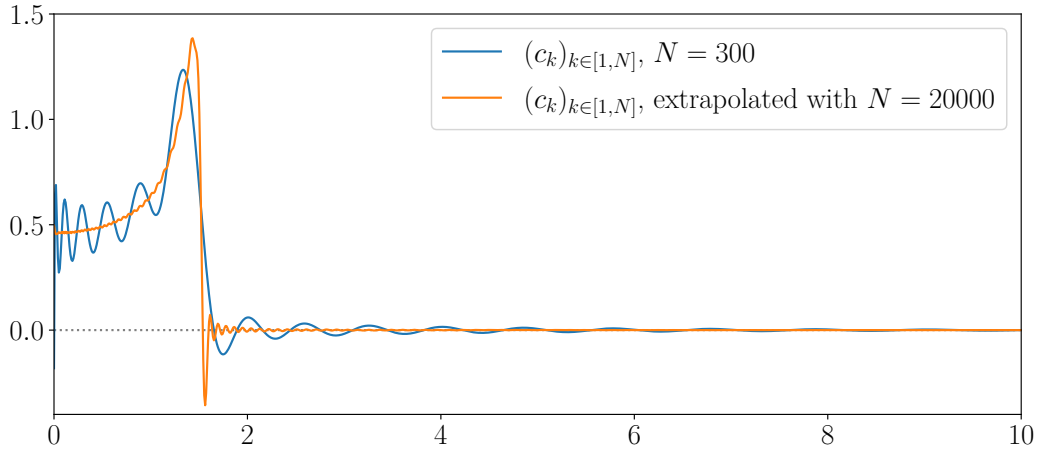
- floating-point operations using 64 bits floats;
- floating-point operations using 128 bits floats;
- SymPy: make the whole computation using SymPy, a Python library of symbolic computation (very slow).

In all three cases, instabilities appear before the sequence $(c_k)_k$ has fully converged to 0. Moreover, the oscillations of $(c_k)_k$ around 0 have an increasing wavelength, which indicates that we may have to go far beyond $k = 500$ to get enough coefficients $(c_k)_k$ to reconstruct the wanted inverse Mellin transform.

In Figure 13, we have plotted two estimations of $f_{|Y|}$: the density obtained directly by using $(c_k)_{k \in [1, 300]}$, and the density obtained by using a sequence $(c_k)_{k \in [1, 20000]}$ where the values $(c_k)_{k \in [301, 20000]}$ have been extrapolated from $(c_k)_{k \in [1, 300]}$.²²

The resulting estimations of the density $f_{|Y|}$ take negative values and seem to be noised. So, more work is needed to obtain smooth and proper densities, especially if we want them to meet Constraints 3 and 4 (density at 0 and decay rate at ∞).

²²The extrapolation has been performed by modeling the graph of $(c_k)_k$ as the product of a decreasing function and a cosine with decreasing frequency.

Figure 12: Evolution of various numerical computations of c_k as k grows.Figure 13: Numerical inverse Mellin transform with two different computations of $(c_k)_k$: direct computation of $(c_k)_{k \in [1, N]}$ with $N = 300$; extrapolation of $(c_k)_{k \in [301, 20000]}$ from $(c_k)_{k \in [1, 300]}$.

Conclusion. We observe that this computation of the inverse Mellin transform has several intrinsic problems:

- the computation of the c_k coefficients involves a sum of terms with alternating signs, which become larger (in absolute value) as k grows and which are supposed to compensate such that $c_k \rightarrow 0$ as $k \rightarrow \infty$. Such a numerical computation, involving both large and small terms, makes the resulting c_k very unstable as k grows;
- when $\theta \approx 2$, the sequence $(c_k)_k$ tends extremely slowly to 0;
- if we approximate $\mathcal{M}^{-1}f$ with the finite sum of the first K terms of the series in Equation (58), we cannot guarantee the non-negativeness of the resulting function, which is meant to be a density.

So, this method is unpractical to compute the density of a distribution in our case.

F Obtaining $f_{|Y|}$: experimental details

We optimize the vector of parameters Λ with respect to the following loss:

$$\begin{aligned}\ell(\Lambda) &:= \|\hat{F}_\Lambda - F_{|G|}\|_\infty \\ \hat{F}_\Lambda(z) &:= \int_0^\infty F_{|W|}\left(\frac{z}{t}\right) g_\Lambda(t) dt.\end{aligned}$$

Dataset. We build the dataset \mathcal{Z} of size d :

$$\mathcal{Z} = \left\{0, z_{\max} \frac{1}{d-1}, z_{\max} \frac{2}{d-1}, \dots, z_{\max}\right\}.$$

In our setup, $d = 200$ and $z_{\max} = 5$.

Computing the loss. For each z in \mathcal{Z} , we compute numerically $\hat{F}_\Lambda(z)$. Then, we are able to compute $\ell(\Lambda)$. We keep track of the computational graph with PyTorch, in order to backpropagate the gradient and train the parameters Λ by gradient descent.

Initialization of the parameters. We initialize $\Lambda = (\alpha, \gamma, \lambda_1, \lambda_2)$ in the following way: $\alpha = 3; \gamma = 1; \lambda_1 = 1; \lambda_2 = 1$.

Optimizer. We use the Adam optimizer (Kingma & Ba, 2015) with the parameters: learning rate = 0.001; $\beta_1 = 0.9$; $\beta_2 = 0.999$; weight decay = 0. We train Λ for 100 epochs.

Learning rate scheduler. We use a learning rate scheduler based on the reduction of the training loss. If the training loss does not decrease at least by a factor 0.01 for 20 epochs, then the learning rate is multiplied by a factor $1/\sqrt[3]{10}$. After a modification of the learning rate, we wait at least 20 epochs before any modification.

Scheduler for θ' . We recall that the definition of g_Λ involves θ' , defined by: $\frac{1}{\theta} + \frac{1}{\theta'} = \frac{1}{2}$. It is not a parameter to train. Empirically, we found that the following schedule improves the optimization process:

- from epoch 0 to epoch 49, θ' increases linearly from 2 to its theoretical value $(\frac{1}{2} - \frac{1}{\theta})^{-1}$;
- at the beginning of epoch 50, we reinitialize the optimizer and the learning rate scheduler;
- we finish the training normally, with $\theta' = (\frac{1}{2} - \frac{1}{\theta})^{-1}$.

G The Kolmogorov–Smirnov test

Description. We describe here the Kolmogorov–Smirnov (KS) test (Kolmogoroff, 1941, Smirnov, 1948). Given a sequence (Z'_1, \dots, Z'_s) of s i.i.d. random variables sampled from P' :

1. we build the empirical CDF F_s of this sample: $F_s(z) = \frac{1}{s} \sum_{k=1}^s \mathbb{1}_{Z'_k \leq z}$;
2. we compare F_s to the CDF F_G of $G \sim \mathcal{N}(0, 1)$ by using the \mathcal{L}^∞ norm: $D_s = \|F_s - F_G\|_\infty$, where D_s is the “KS statistic”;
3. under the null hypothesis, i.e. $P' = \mathcal{N}(0, 1)$, we have: $\sqrt{s}D_s \xrightarrow{d} K$, where K is the Kolmogorov distribution (Smirnov, 1948). We denote by $(K_\alpha)_\alpha$ the quantiles of K : $\mathbb{P}(K \leq K_\alpha) = 1 - \alpha$, for all $\alpha \in [0, 1]$;
4. finally, we reject the null hypothesis at level α if: $\sqrt{s}D_s \leq K_\alpha$.

Limitations. In the KS test presented above, the null hypothesis \mathbb{H}_0 is $P' = \mathcal{N}(0, 1)$, which is exactly what we intend to demonstrate when using our family $\{(P_\theta, \phi_\theta^{\circ/p}) : \theta \in (2, \infty)\}$, while the alternative hypothesis \mathbb{H}_1 is $P' \neq \mathcal{N}(0, 1)$. With this test design, we face a problem: it is impossible to claim that \mathbb{H}_0 holds. More precisely, we have two possible outcomes: either \mathbb{H}_0 is rejected, or it is not. Since \mathbb{H}_1 is the complementary of \mathbb{H}_0 , a reject of \mathbb{H}_0 means an accept of \mathbb{H}_1 . But the converse does not hold: if \mathbb{H}_0 is not rejected, then it is impossible to conclude that \mathbb{H}_0 is true: the sample size s may simply be too small, or the KS test may be inadequate for our case.

So, to be able to conclude that the pre-activations are Gaussian, we should have built an alternative test, where the null hypothesis \mathbb{H}'_0 is some *misfit* between P' and $\mathcal{N}(0, 1)$. Or, at least, we should have computed the power of the current KS test.

However, our experimental results are sufficient to *compare* the quality of fit between P' and $\mathcal{N}(0, 1)$ in the tested setups (see Figures 6 and 7). It remains clear that, with $\{(P_\theta, \phi_\theta) : \theta \in (2, \infty)\}$, the Gaussian pre-activations hypothesis is far more likely to hold than in setups involving tanh, ReLU and Gaussian weights.

H Experiments

H.1 Propagation of the correlations with MNIST

Within the setup of Section 3.2, we have plotted in Figure 14 the correlations propagated in a multilayer perceptron with inputs sampled for MNIST (10 samples per class, that is, 100 samples in total). The layers of the perceptron have $n_l = 10$ neurons each, and the activation function is $\phi = \text{ReLU}$.

We observe that, in this narrow NN case ($n_l = 10$), some irregularities appear as information propagates into the network: some classes seem to (de)correlate in an inconsistent way with the others. Specifically, while most of the classes tend to correlate exactly ($C^* \approx 1$), the third class (corresponding to the digit “2”) tends to a correlation $C^* \approx 0.7 \neq 1$. This result is contradictory to the EOC theory.

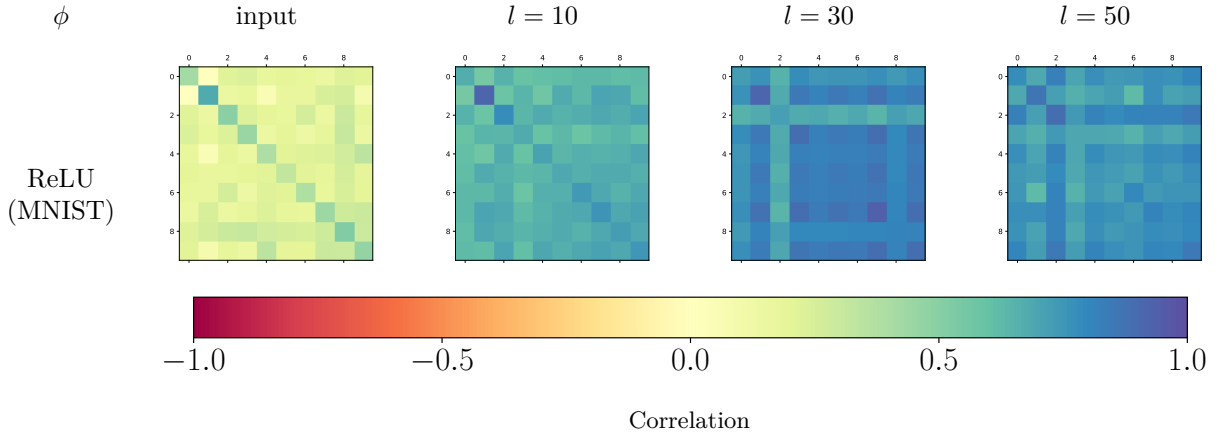


Figure 14: Propagation of correlations c_{ab}^l in a multilayer perceptron with activation function $\phi = \text{ReLU}$ and inputs sampled from the MNIST dataset. The neural network is initialized at the EOC. Each plot displays a 10×10 matrix C_{pq}^l whose entries are the average correlation between the pre-activations propagated by samples from classes $p, q \in \{0, \dots, 9\}$, at the input and right after layers $l \in \{10, 30, 50\}$. See also Figure 1 in Section 3.2 for results on CIFAR-10.

H.2 Propagation of the correlations with $\phi = \phi_\theta^\circ$

Within the setup of Section 3.2, we have plotted in Figure 15 the correlations propagated in a multilayer perceptron with $\phi = \phi_\theta$. The weights have been sampled from $\mathcal{W}(\theta, 1)$.

In this setup, the results are consistent, and are consistent with the results for $\phi = \tanh$ (see Figure 1): the sequence $(C_{pq}^l)_l$ converges to 1, which was not the case for $\phi = \text{ReLU}$ and $n_l = 10$.

H.3 Variance of the pre-activation when using $\phi = \phi_\theta^\circ$

As observed in Figure 6a, the product $W\phi_\theta(X)$ is above the KS threshold, corresponding to $s = 10^7$ samples and a p -value of 0.05. This is not necessarily the case in Figure 6b, where the samples are standardized. So, we suspect that the variance of $W\phi_\theta^\circ(X)$ is not exactly 1.

Therefore, we have reported in Table 2 the empirical standard deviation of the product $W\phi(X)$ (i.e., Z' with $n = 1$), computed with $s = 10^7$ samples, where $X \sim \mathcal{N}(0, 1)$, $W \sim \mathcal{W}(\theta, 1)$ if $\phi = \phi_\theta$ and $W \sim \mathcal{N}(0, 1)$ if $\phi = \tanh$ or ReLU . We observe that the standard deviation of Z' , which is expected to be 1 with $\phi = \phi_\theta^\circ$, is actually a bit different. This would largely explain the differences between Figure 6a and Figure 6b.

Table 2: Empirical standard deviation of Z' with $n = 1$.

	ϕ_θ°							\tanh	ReLU
θ	2.05	2.5	3	4	5	7	10		
$\bar{\sigma}$	1.003	0.994	0.989	0.984	0.981	0.979	0.978	0.628	0.707

H.4 Propagation of the pre-activations

In this subsection, we show how the choice of the input data points affect the propagation of the pre-activations.

Let \mathcal{D}^l be the distribution of the pre-activation Z_1^l after layer l . In Figure 16, we have plotted the \mathcal{L}^∞ distance between the CDFs of \mathcal{D}^l and $\mathcal{N}(0, 1)$ for various input points, sampled from different classes to improve diversity between them. We have chosen the following setup: CIFAR-10 inputs, multilayer perceptron with 100 layers and 100 neurons per layer, Gaussian initialization at the EOC when using the activation function $\phi = \tanh$ or ReLU , and symmetric Weibull initialization $\mathcal{W}(\theta, 1)$ when using $\phi = \phi_\theta^\circ$ or $\phi = \phi_\theta^p$.

This setup has been selected to illustrate clearly the variability of \mathcal{D}^l when using various data points. This variability can be observed with 10 or 1000 neurons per layer, though it is less striking.

Input normalization over the whole dataset. We perform the usual normalization over the whole dataset:

$$\begin{aligned}\hat{x}_{a;ij} &:= \frac{x_{a;ij} - \mu_i}{\sigma_i}, \\ \mu_i &:= \frac{1}{Np_i} \sum_{\mathbf{x} \in \mathbb{D}} \sum_{j=1}^{p_i} x_{ij} \\ \sigma_i^2 &:= \frac{1}{Np_i - 1} \sum_{\mathbf{x} \in \mathbb{D}} \sum_{j=1}^{p_i} (x_{ij} - \mu_i)^2,\end{aligned}$$

where $\hat{\mathbf{x}}$ is the normalized data point, $x_{a;ij}$ is the j -th component of the i -th channel of the input image \mathbf{x}_a , p_i is the size of the i -th channel, and N is the size of the dataset \mathbb{D} .

Results. In Figure 16, we observe that, when using the activation function $\phi = \tanh$, the shape of the curves is the same for all data points. This is not the case for ReLU : for the input point “bird”, the sequence $(\mathcal{D}^l)_l$ drifts away from $\mathcal{N}(0, 1)$ since the beginning, while for the input “car”, $(\mathcal{D}^l)_l$ first becomes closer to $\mathcal{N}(0, 1)$, then drifts away. It is also the case for ϕ_θ with $\theta = 10$: for the input “deer”, the distance remains high, while it starts low and increases very slowly (input “dog”), or even decreases in the first place (input

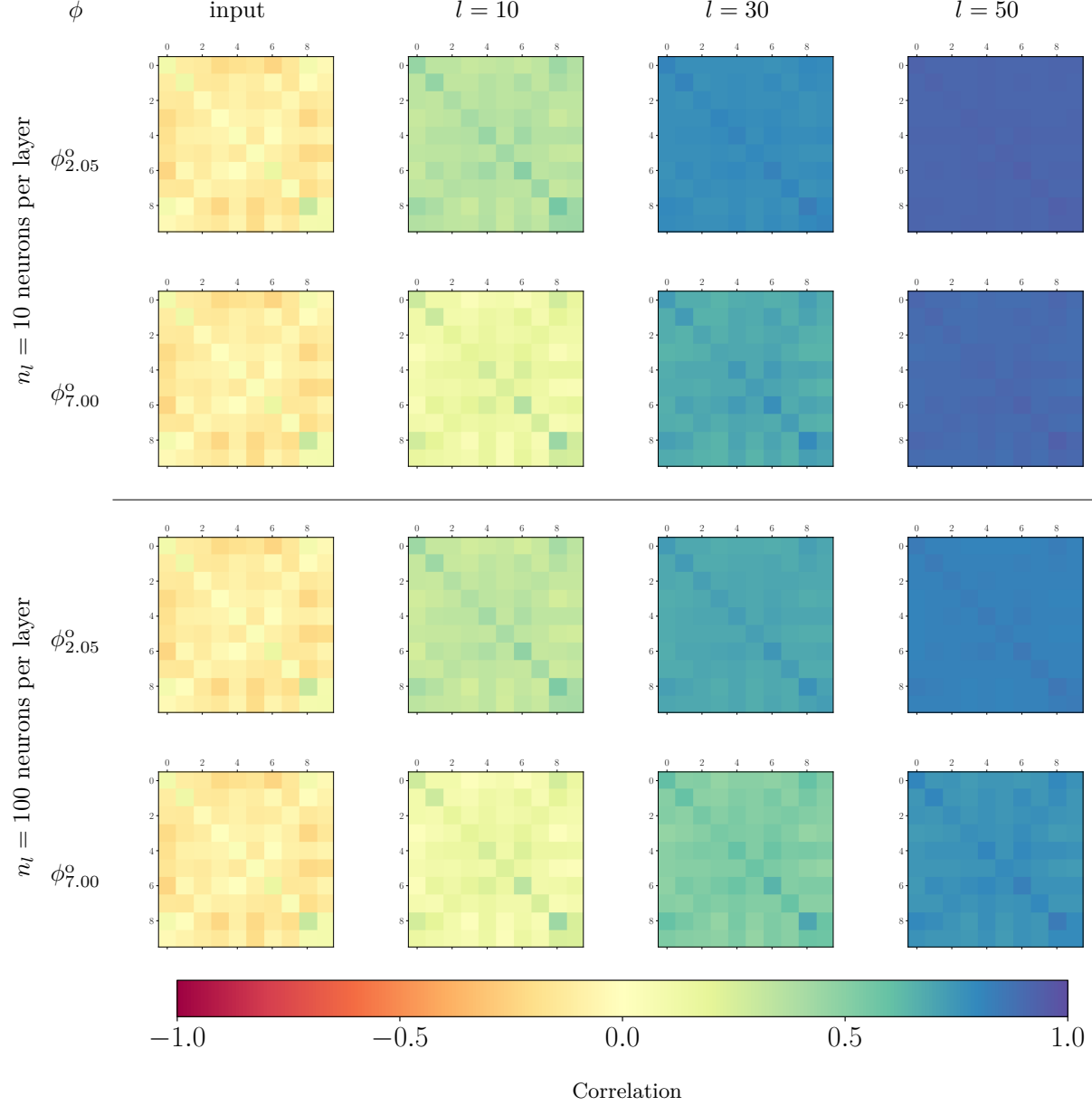


Figure 15: Propagation of correlations c_{ab}^l in a multilayer perceptron with activation function ϕ_θ^o with $\theta \in \{2.05, 7.00\}$ and inputs sampled from the CIFAR-10 dataset. The weights are sampled from $\mathcal{W}(\theta, 1)$ and the biases are zero. Each plot displays a 10×10 matrix C_{pq}^l whose entries are the average correlation between the pre-activations propagated by samples from classes $p, q \in \{0, \dots, 9\}$, at the input and right after layers $l \in \{10, 30, 50\}$.

“truck”). But, in general, when the curves have converged after 100 layers, it seems that the limit is the same whatever the starting data point, and depends only on the choice of the activation function.

The most striking result lies in the difference between Figures 16 and 17. With $\phi = \phi_\theta^p$, the pre-activations tend *always to be Gaussian*, whatever θ or the input data point. This is not the case with ReLU, tanh and some ϕ_θ^p with large θ . However, ϕ_θ^p remain “more Gaussian” than ReLU or tanh.

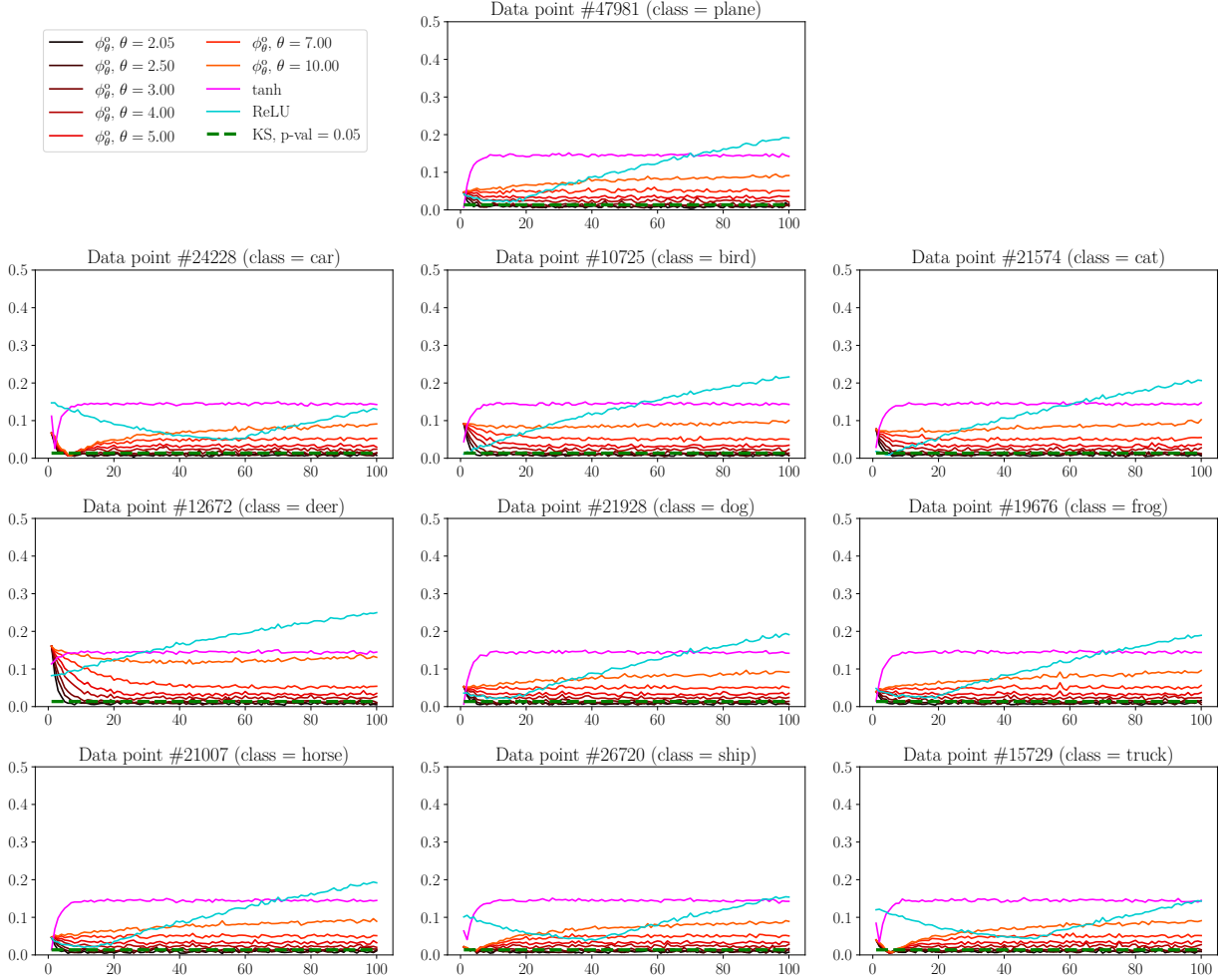
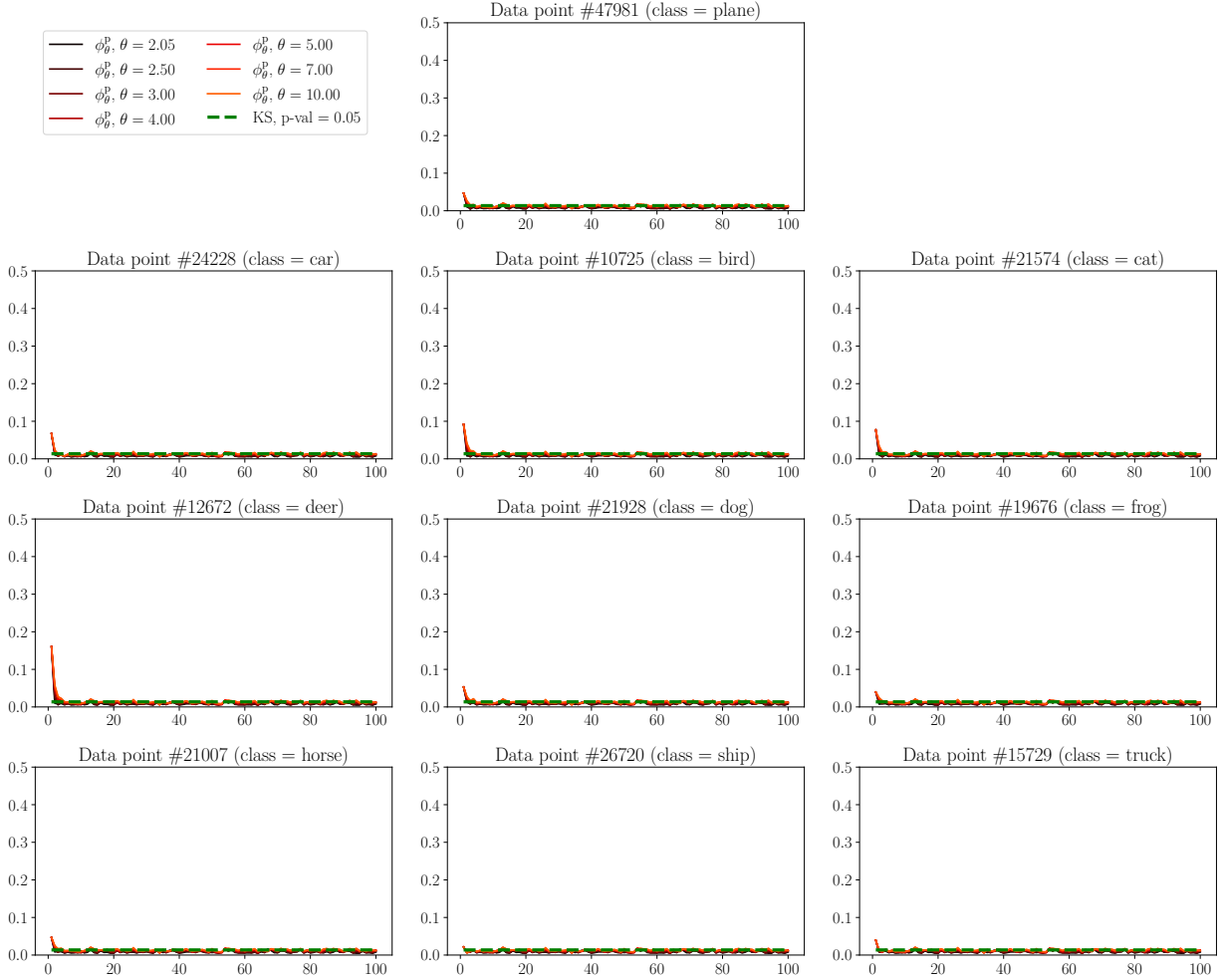


Figure 16: Activations functions tanh, ReLU and ϕ_θ^o .

Propagation of the distribution \mathcal{D}^l of the pre-activations across the layers $l \in [1, 100]$ when inputting various data points of CIFAR-10. Each curve represents the \mathcal{L}^∞ distance between the CDF of \mathcal{D}^l and the CDF of the Gaussian $\mathcal{N}(0, 1)$. The dashed green line is the threshold of rejection of the Kolmogorov–Smirnov test with p -value 0.05: if a distribution \mathcal{D}^l is represented by a point above this threshold, then the hypothesis “ $\mathcal{D}^l = \mathcal{N}(0, 1)$ ” is rejected with p -value 0.05.

Figure 17: Activation functions ϕ_{θ}^p , same setup as in Figure 16.

H.5 Experimental details of the training procedure

Training, validation, and test sets. For MNIST and CIFAR-10, we split randomly the initial training set into two sets: the training set, which will be actually used to train the neural network, and the validation set, which will be used to stop training when the network begins to overfit.

The sizes of the different sets are as follows:

- MNIST: 50000 training samples; 10000 validation samples; 10000 test samples;
- CIFAR-10: 42000 training samples, 8000 validation samples; 10000 test samples.

The training sets are split into mini-batches with 200 samples each. No data augmentation is performed.

Loss. Given a classification task with P classes, let $\mathbf{z}^L \in \mathbb{R}^P$ be the pre-activation outputted by the last layer of the neural network. First, we perform a softmax operation:

$$y_p := \text{softmax}(z_p^L) = \frac{\exp(z_p^L)}{\sum_{p'=1}^P \exp(z_{p'}^L)}.$$

where the $(y_p)_p$ are the components of $\mathbf{y} \in \mathbb{R}^P$ and $(z_p^L)_p$ are the components of \mathbf{z}^L . Then, we compute the negative log-likelihood loss. For a target class $p \in \{1, \dots, P\}$, we pose:

$$\ell(\mathbf{y}, p) := -\log(y_p).$$

Optimizer. We use the Adam optimizer (Kingma & Ba, 2015) with the parameters: learning rate = 0.001; $\beta_1 = 0.9$; $\beta_2 = 0.999$; weight decay = 0.

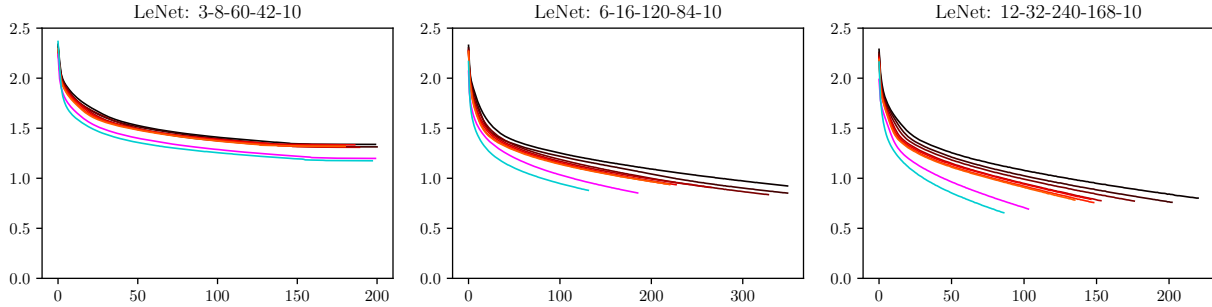
Learning rate scheduler. We use a learning rate scheduler based on the reduction of the training loss. If the training loss does not decrease at least by a factor 0.01 for 10 epochs, then the learning rate is multiplied by a factor $1/\sqrt{10}$.

Early stopping. We add an early stopping rule based on the reduction of the validation loss. If the validation loss does not decrease at least by a factor of 0.001 for 30 epochs, then we stop training.

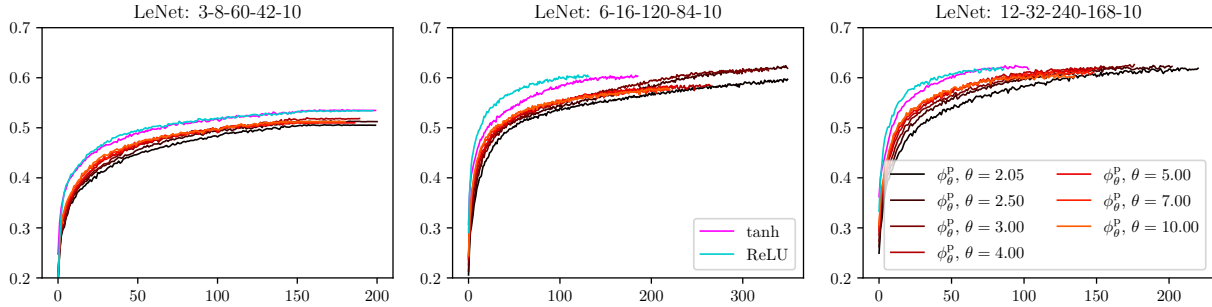
H.6 Additional training results: $\phi = \phi_\theta^p$

We provide here additional training experiments, with the same setup as in Section 5.4 but with our family of positive activation functions $(\phi_\theta^p)_\theta$.

Results with CIFAR-10 + LeNet. We have plotted in Figure 18 the evolution of the training loss and the test accuracy during training. The test loss is slightly better than with the family of odd activation functions $(\phi_\theta^o)_\theta$ (see Fig. 9b) and the training loss is slightly worse (see Fig. 9a). Overall, the plots are very similar with both types of activations functions.



(a) Training loss (negative log-likelihood).



(b) Test accuracy.

Figure 18: Training curves for CIFAR-10 + LeNet with 3 different numbers of neurons per layer and $\phi = \phi_\theta^p$.

Results with MNIST + Multilayer perceptron. We have plotted in Figure 19 the results of the training of a narrow multilayer perceptron, as in Figure 10. In this extreme setup, the positive activation functions ϕ_θ^p perform worse than the odd ones ϕ_θ^o . In particular, many trainings failed with a narrow and deep network ($L = 30$).

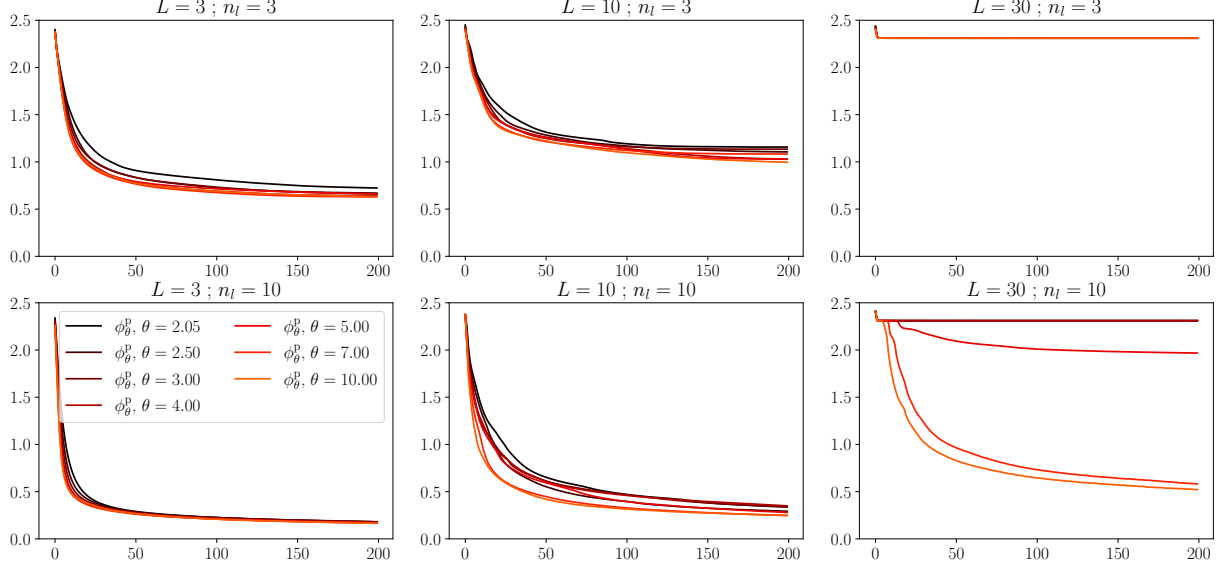


Figure 19: Training loss for a multilayer perceptron, narrow ($n_l \in \{3, 10\}$) and of various depths ($L \in \{3, 10, 30\}$). Training curves averaged over 5 experiments.